HHS Public Access

Author manuscript

Prog Biophys Mol Biol. Author manuscript; available in PMC 2016 January 22.

Published in final edited form as:

Prog Biophys Mol Biol. 2015 January ; 117(1): 43–58. doi:10.1016/j.pbiomolbio.2015.01.003.

Mathematical modeling of acid-base physiology

Rossana Occhipinti[a,*] and **Walter F. Boron**[a,b]

[a] Department of Physiology and Biophysics, Case Western Reserve University School of Medicine, Cleveland, OH 44106, USA

[b] Department of Medicine, Case Western Reserve University School of Medicine, Cleveland, OH 44106, USA

Abstract

pH is one of the most important parameters in life, influencing virtually every biological process at the cellular, tissue, and whole-body level. Thus, for cells, it is critical to regulate intracellular pH (pH_i) and, for multicellular organisms, to regulate extracellular pH (pH_o). pH_i regulation depends on the opposing actions of plasma-membrane transporters that tend to increase pH_i, and others that tend to decrease pH_i. In addition, passive fluxes of uncharged species (e.g., CO_2, NH_3) and charged species (e.g., HCO_3^- , NH_4^+) perturb pH_i. These movements not only influence one another, but also perturb the equilibria of a multitude of intracellular and extracellular buffers. Thus, even at the level of a single cell, perturbations in acid-base reactions, diffusion, and transport are so complex that it is impossible to understand them without a quantitative model. Here we summarize some mathematical models developed to shed light onto the complex interconnected events triggered by acids-base movements. We then describe a mathematical model of a spherical cell–which to our knowledge is the first one capable of handling a multitude of buffer reaction–that our team has recently developed to simulate changes in pH_i and pH_o caused by movements of acid-base equivalents across the plasma membrane of a *Xenopus* oocyte. Finally, we extend our work to a consideration of the effects of simultaneous CO_2 and HCO_3^- influx into a cell, and envision how future models might extend to other cell types (e.g., erythrocytes) or tissues (e.g., renal proximal-tubule epithelium) important for whole-body pH homeostasis.

Keywords

Reaction-diffusion; Whole-body; Epithelia; Cell; Competing equilibria

1. Introduction

The field of acid-base physiology has advanced significantly in recent years, thanks to the rapid accumulation of molecular biological insight–including genome-sequence data–as well as functional, biochemical, and cell biological studies. Progress with in-vitro expression systems (e.g., *Xenopus* oocytes, cells in culture) and genetically manipulated animals has

* Corresponding author. Department of Physiology and Biophysics, Case Western Reserve University School of Medicine, 10900 Euclid Avenue , Cleveland, OH 44106, USA. Tel.: +1 216 368 3631; fax: +1 216 368 5586. rossana.occhipinti@case.edu (R. Occhipinti)..

produced a large amount of new data. In spite of significant progress, we are still far from fully understanding the mechanisms involved in acid-base homeostasis. For example, we are still unable to discern with certainty the relative contribution of the many simultaneous and interconnected processes (e.g., movements of numerous acid-base equivalents, equilibria of a multitude of buffers) that produce pH changes in a single living cell, let alone a tissue or the whole organism.

Understanding acid-base physiology is important because virtually every biological process is pH sensitive. Perturbations in pH can affect a variety of biological processes at the cellular, tissue, and whole-body level. At the cellular level, maintaining cytosolic pH (i.e., intracellular pH, pH_i) within a narrow range is essential for many processes to occur, including biochemical reactions, as well as the function of transporters, channels, receptors, structural proteins, and regulatory molecules (Ludwig et al., 2003; Roos and Boron, 1981; Waldmann et al., 1997). In addition, pH_i influences the luminal pH of membrane-bound intracellular organelles (e.g., endoplasmic reticulum, endosomes, mitochondria), and thereby has an indirect influence on the myriad events occurring inside these organelles (Igawa et al., 2010; Matsuyama and Reed, 2000; Roopenian and Akilesh, 2007). At the tissue level, local extracellular pH (pH_o) not only influences pH_i (Boron, 2012a; Roos and Boron, 1981) but also modulates the binding of extracellular ligands to cell-surface receptors (Roopenian and Akilesh, 2007), and a host of regional processes that include blood flow (Boedtkjer and Aalkjær, 2012), air flow in the lungs (Duckles et al., 1974; Kolobow et al., 1977; Winn et al., 1983), maintenance of appropriate corneal hydration and transparency (Li et al., 2005; Sun and Bonanno, 2003), epithelial transport, and the binding of ligands to extracellular receptors (Traynelis, 1998). At the whole-body level, the pH of blood plasma not only influences local tissue pH_o (which in turn affects pH_i) but also modulates interactions, in the plasma, of charged molecules (e.g., hormones and their carrier proteins). In the realm of patient care, plasma pH affects the electrical charge of therapeutic agents that are weak acids or weak bases, and how these agents interact with plasma proteins and distribute among the tissues (Rodgers and Rowland, 2006; Rodgers et al., 2005).

Because pH changes have such profound effects on biology, organisms have evolved a series of sophisticated mechanisms to achieve homeostasis of pH in the intracellular fluid, blood plasma, and other compartments in the body. The process by which cells or the whole body respond to perturbations in pH by tending to return pH to its initial value is known as “pH regulation”. Regulation of pH in the blood plasma–and, by extension, in the extracellular fluid-–is the result of the dual action of the respiratory and renal systems, which independently control the concentrations of carbon dioxide (CO_2) and bicarbonate (HCO_3^-), the two major components of the body's most important buffering system. More specifically, the lungs regulate plasma [CO_2], whereas the kidneys, plasma [HCO_3^-].

Cells regulate pH_i by appropriately adjusting the speeds of various transporters that move acids (including hydrogen ions or protons, H^+) or bases (e.g., HCO_3^-) across the plasma membrane. The movements across the membrane of uncharged weak acids or bases (e.g., butyric acid or ammonia, NH_3), or of their charged counterparts (e.g., butyrate or ammonium, NH_4^+), can produce pH_i perturbations against which cells defend themselves using their pH_i-regulatory machinery.

Movements of acid-base equivalents across the plasma membrane–whether these movements are the insults that perturb pH_i or the regulatory response–influence one another and alter the equilibria of numerous intracellular and extracellular buffers, thereby creating complicated interdependencies among acid-base reactions, diffusion, and carrier-mediated transport. Because of the complexity of such movements, several investigators have developed mathematical models of acid-base physiology to help in data interpretation.

In this review, first we provide an overview of acid-base physiology with special emphasis to the mechanisms of pH regulation in the body and cell. Then, we summarize mathematical models of acid-base physiology by others. Finally, we summarize the most recent models from our team.

2. Overview of acid-base physiology

2.1. Acid-base chemistry

Before reviewing how the body, tissues and cells achieve pH homeostasis, it is useful to draw our attention to the most powerful buffering system[1] in the body–the CO_2/HCO_3^- buffer pair.

Dissolved CO_2, HCO_3^-, and H^+ are related through the reactions

$$CO_2 + H_2O \rightleftharpoons H_2CO_3 \rightleftharpoons HCO_3^- + H^+. \quad (1)$$

The first step of these reactions, the CO_2 hydration reaction, is extremely slow. To meet physiological needs, virtually all cells and tissues express a form of the enzyme carbonic anhydrase (CA), which catalyzes (or, more accurately, bypasses) this slow reaction. The second step of reactions (1), the dissociation of carbonic acid (H_2CO_3), is extremely fast. Thus, in the absence of CA, the slow CO_2 hydration reaction is the limiting step in the conversion of CO_2 into HCO_3^- and H^+, and vice versa.

Ignoring the H_2CO_3 intermediate in reaction (1), we can write the thermodynamically equivalent form

$$CO_2 + H_2O \rightleftharpoons HCO_3^- + H^+. \quad (2)$$

The equilibrium constant for this reaction is

$$K = \frac{[HCO_3^-]\,[H^+]}{[CO_2]},$$

which, in logarithmic form, can be written as

[1] A buffer is any substance that tends to minimize changes in pH by reversely producing or consuming H^+.

$$pH = \mathrm{p}K + log_{10}\frac{[HCO_3^-]}{[CO_2]}. \quad (3)$$

This is the Henderson–Hasselbalch (Hasselbalch, 1916; Henderson, 1908; Sendroy et al., 1934) equation which states that, in a simple CO_2/HCO_3^- buffer system, it is not these two individual buffer components that determine pH, but their ratio.

Recalling that, according to Henry's law, dissolved $[CO_2] = s \cdot P_{CO2}$, where s is the solubility coefficient of CO_2 and P_{CO2} is the partial pressure of CO_2, we can rewrite Equation (3) in the form

$$pH = \mathrm{p}K + log_{10}\frac{[HCO_3^-]}{s \cdot \mathrm{P}_{CO_2}}. \quad (4)$$

Substituting into Equation (4) reasonable values for the p*K* of the CO_2/HCO_3^- equilibrium (e.g., 6.1), $[HCO_3^-]$ (e.g., 24 mM), the solubility of CO_2 (e.g., 0.03 mM/mm Hg), and P_{CO2} (e.g., 40 mm Hg), we see that the Henderson–Hasselbalch equation correctly predicts a pH of ~7.40 for normal, human arterial blood at 37 °C (Boron, 2012a).

The CO_2/HCO_3^- buffer system is the most important buffer in the body for three reasons. First, the body independently and appropriately regulates $[CO_2]$ and $[HCO_3^-]$ in response to changes in the acid-base status of the blood. Second, the sum $[CO_2] + [HCO_3^-]$ is higher than for any other buffer pair. And third, the body behaves as an open system for CO_2. Fig. 1 illustrates the pH dependence of buffering power (i.e., the amount of strong base per unit volume of solution necessary to produce a given increase in pH) of the CO_2/HCO_3^- buffer in a fluid having the composition of normal arterial blood. If the system is “closed” with respect to CO_2/HCO_3^- – that is, neither of its components can communicate with the environment (e.g., it is contained in a closed syringe with no gas phase)–its buffering power has a bell-shaped dependence on pH and reaches its maximum value when pH is equal to p*K*. If the system is “open” with respect to CO_2–that is, $[CO_2]$ is stabilized by communication with the environment (e.g., it is contained in a beaker where the CO_2 can exchange with the overlying air)–the buffering power of the CO_2/HCO_3^- buffer pair rises exponentially with pH. Thus, for a closed-system buffer, buffering power (β)–a measure of the ability of the buffer to resist to changes in pH–is greatest in the pH range close to the p*K*, whereas for an open-system buffer, the effectiveness of the buffer increases with pH.

If the system were closed for CO_2/HCO_3^- , the maximal CO_2/ HCO_3^- buffering power (i.e., at pH p*K* 6.1) would be modest (Fig. 1), and its buffer power at the physiological blood-plasma pH of 7.4 would be quite small (Davenport, 1974; Seldin and Giebisch, 1989). The great potency of the CO_2/HCO_3^- buffer in the blood derives from the system's being open for CO_2, which can continuously exit or enter the blood plasma across the alveolar blood-gas barrier, thereby achieving a near equality between the P_{CO2} in alveolar air and the P_{CO2} in arterial blood. Because alveolar ventilation maintains a stable P_{CO2} in the alveolar air, this system maintains a stable $[CO_2]$ in arterial blood plasma, as well. Moreover, the respiratory

system can regulate ventilation to stabilize arterial [CO_2] when CO_2 production changes (e.g., during exercise), or regulate ventilation to achieve a shift in alveolar P_{CO2} to compensate for an acid-base disturbances.

2.2. Whole-body pH regulation

The human body is challenged daily with a continuous production of CO_2 and far smaller amounts of strong acids (Giebisch and Windhager, 2012). An adult on a "typical Western diet" produces ~15,000 mmol/day of CO_2 via metabolism (Giebisch and Windhager, 2012). The respiratory system uses very efficient mechanisms (e.g., diffusion and convection) to remove from the blood this CO_2 that otherwise would acidify all the extra- and intracellular fluids by forming H^+ through reaction (2). In addition to CO_2, metabolism produces ~40 mmol/day of non-volatile acids that, together with ~20 mmol/day of strong acid contained in a "typical Western diet" and the obligatory intestinal loss of ~10 mmol/day of alkali, represents a total net load of ~70 mmol/day of non-volatile acids (Giebisch and Windhager, 2012). As the 70 mmol/day of non-volatile acids appear in the extracellular fluid, extracellular HCO_3^- neutralizes these acids by forming CO_2 and H_2O.[2] 2 Thus, the appearance of ~70 mmol/day of non-volatile acids in the extracellular fluid (ECF) corresponds to the disappearance of an equal amount of HCO_3^- from the ECF.[3] The kidneys reverse this process by excreting ~70 mmol/day of H^+ into the urine and simultaneously transporting ~70 mmol/day of "new" HCO_3^- into the blood plasma, thereby regenerating the extracellular HCO_3^- that was consumed during the neutralization of the non-volatile acids. In so doing, the kidneys maintain blood [HCO_3^-] constant and prevent the blood from acidifying.

In the remainder of this section, we will review how the respiratory system controls blood [CO_2] and how the renal system control blood [HCO_3^-], thereby maintaining the blood pH in the normal physiological range.

2.2.1. The respiratory system—Fig. 2 provides an overview of the human respiratory system, and how it removes CO_2 from the body, using a combination of diffusion and convection (Boron, 2012b). CO_2 originates in the mitochondria as a result of aerobic metabolism. Because P_{CO2} is highest in the mitochondria, CO_2 *diffuses* down its concentration gradient from the cell to the extracellular space, and then into the systemic capillaries. Here, ~10% of the total CO_2 remains in the blood plasma, whereas the remaining ~90% enters the red blood cells (RBCs), where most of it undergoes the reaction $CO_2 + H_2O \rightarrow HCO_3^- + H^+$, catalyzed by CA I and II. Hemoglobin (Hb) buffers the newly produced H^+, thereby playing an important role in acid-base chemistry. Simultaneously, the Cl–HCO_3 exchanger AE1 exports the newly formed HCO_3^- (Jennings, 1989; Parker and Boron, 2013). Thus, RBCs are the key to CO_2 carriage in the blood. Following these diffusion and transport events, it is the *internal convective system* that carries the CO_2-rich blood from the systemic capillaries to the pulmonary capillaries (Boron, 2012c). Thanks to its separate right and left hearts that, respectively, drive blood through the separate

[2]The CO_2 produced in this process is removed by the lungs.
[3]In reality, a small amount of non-volatile acids is neutralized by non CO_2/HCO_3^- buffers which are also present in the blood.

pulmonary and systemic circulations, the circulatory system delivers blood with high P_{CO2} to the pulmonary capillary. The result is a maximization of the CO_2 concentration gradient that now drives the *diffusion* of CO_2 across the capillary endothelium and alveolar epithelium into the alveolar air space in the lungs. Finally, the *external convective system*, the ventilatory machinery or air pump–consisting of the chest wall, the respiratory muscles and the conduits for the airflow–moves the CO_2-rich air from the alveolar space to the atmosphere, and moves O_2-rich ambient air in the opposite direction. This exchange of alveolar and ambient air, or *alveolar ventilation*, is under the control of the central nervous system, which sets the depth and frequency of ventilation, and appropriately modulates both in response to changes in arterial P_{O2}, P_{CO2}, and pH.

In summary, the respiratory system uses diffusion for the short-distance movements of CO_2 near the systemic and pulmonary capillaries, and convection for the long-distance movements of CO_2 from the systemic to the pulmonary capillaries and again from the alveoli to the environment.

2.2.2. The renal system—As already noted, the kidneys create and transfer to the blood an amount of new HCO_3^- that is equal to the sum of non-volatile acids produced by metabolism plus non-volatile acids assimilated from the diet plus base lost to the GI tract. However, before the kidneys can perform this task–known as HCO_3^- generation–they must retrieve from the nephron lumen all ~4500 mmol of HCO_3^- that the glomeruli filter each day, and that otherwise would be lost in the urine (Giebisch and Windhager, 2012; Seldin and Giebisch, 1989). Fig. 3 illustrates the basic cellular mechanism of this proces–known as HCO_3^- reabsorption–which occurs slightly differently at three sites along the nephron. The major site is the proximal tubule, which reclaims ~80% of the filtered HCO_3^- .

As the tubule cells secrete H^+ into the tubule lumen, the H^+ titrates the HCO_3^- filtered in the glomerulus, ultimately forming CO_2 and H_2O. The newly formed CO_2 and H_2O diffuse into the tubule cell, where they regenerate intracellular H^+ and HCO_3^- via the action of cytosolic CA II. This H^+ then recycles back into the lumen, whereas the HCO_3^- moves out of the tubule cell across the baso-lateral membrane, and into the interstitial space and ultimately in the blood. Thus, for each H^+ secreted in the tubule lumen, one HCO_3^- disappears from the lumen and one appears in the blood.

We have already mentioned that the other acid-base function of the kidney is to create the new HCO_3^- that replaces the HCO_3^- consumed by neutralizing the daily load of non-volatile acids. This creation of new HCO_3^- occurs when the H^+ secreted into the tubule lumen combines with buffers other than HCO_3^- . When the H^+ titrates urinary buffers other than HCO_3^- or NH_3, the process is known as titratable acid formation. When the H^+ titrates NH_3 (of if the cell actually secretes NH_4^+), the process is known as ammonium excretion.

Fig. 4A illustrates the mechanisms underlying titratable acid formation. The H^+ secreted into the tubule lumen combines with a urinary buffer (A^-)–such as phosphate, creatinine, or urate–and then is excreted via the urine. In parallel, one intracellular HCO_3^- forms and moves to the interstitial space via a transport mechanism located at the basolateral

membrane of the tubule cell. Thus, for each H^+ secreted into the tubule lumen, one "new" HCO_3^- appears in the blood.

Fig. 4B illustrates the mechanisms underlying ammonium secretion. Metabolism of glutamine in the proximal tubule produces NH_4^+ and OH^- in the cytosol (Giebisch and Windhager, 2012). NH_4^+ dissociates into NH_3 and H^+, which then move into the tubule lumen, where they recombine to form NH_4^+ that is ultimately excreted in the urine. In the cytosol, CA converts the newly formed OH^- and CO_2 into HCO_3^- , which then moves into the interstitial fluid and blood.

Note that with the secretion of H^+ into the lumen, all three processe–HCO_3^- reabsorption, titratable acid formation, and NH_4^+ secretion–occur simultaneously. The extent to which each process occurs depends on the buffering power of each buffer, which in turn depends on luminal pH, the pK of each reaction, and the total concentration of each buffer species.

2.3. Intracellular pH regulation

Control of pH at the whole-body level depends on the control of pH at the level of a single cell and vice versa. Because intracellular processes (sensitive to changes in pH_i) far outnumber extracellular processes (sensitive to changes in pH_o), pH_i regulation has far more direct impact on function.

In this section, we discuss the mechanisms that influence pH_i and that cells use to maintain pH_i in the normal physiological range. For a more exhaustive overview, refer to (Bevensee and Boron, 2013).

2.3.1. Passive fluxes of uncharged weak acids and bases—Processes that can rapidly influence pH_i–though in a self-limited fashion–are the movement of an uncharged weak acid (HA)

$$HA \rightleftharpoons A^- + H^+ \quad (5)$$

or weak base (B)

$$BH^+ \rightleftharpoons B + H^+ \quad (6)$$

across the plasma membrane. The driving force that moves HA or B into or out of the cell is the chemical gradient (i.e., difference in [HA] or [B] between extra- and intracellular fluid).

In the case of an uncharged weak acid, suddenly increasing $[HA]_o$ above $[HA]_i$ would promote a net influx of HA, followed by a dissociation of intracellular HA into A^- and H^+, causing pH_i to fall. The opposite would occur if $[HA]_o$ suddenly decreased below $[HA]_i$ (i.e., pH_i would rise). In the case of either net influx or efflux, the transmembrane movement of HA would continue until $[HA]_i = [HA]_o$, at which point the net flux of HA would halt–provided that HA is the only species that moves across the plasma membrane. These are examples of an acute acid load (in the case of HA influx) or an acute alkali load (in the case of HA efflux). These acid/alkali loads are "acute" in the sense that they are fundamentally

limited: the production or consumption of H^+ continues in a predictable fashion only until $[HA]_i$ $[HA]_o$.

Acetic acid and CO_2 are examples of uncharged species that behaves like HA in the above examples. Note that although CO_2 is often regarded as an acid, in reality it is not. The true weak acid is H_2CO_3, the result of the interaction of CO_2 with H_2O. It is instructive to consider the consequences of suddenly increasing the rate of CO_2 production inside a cell. At first, $[CO_2]_i$ will rise and, via the reaction $CO_2 + H_2O \rightarrow HCO_3^- + H^+$, lead to a fall in pH_i. However, the rise in $[CO_2]_i$ will lead to a progressive increase in the passive efflux of CO_2 from the cell, so that at some point, the increment in CO_2 efflux matches the increment in production, and no further fall in pH_i occurs.

In the case of an uncharged weak base, suddenly increasing (decreasing) $[B]_o$ above (below) $[B]_i$ provokes the opposite series of changes that we saw in the case of increasing (decreasing) $[HA]_o$. Of course, the influx (efflux) of B causes an acute or self-limited alkali (acid) load.

NH_3 is an example of uncharged weak base that behaves like B in the above example. That is, transmembrane NH_3 fluxes cause pH_i to rise or fall depending on whether $[NH_3]_o$ is higher or lower than $[NH_3]_i$.

The preceding discussion makes no statement about the mechanism by which HA or B passively cross the cell membrane. Although the classic view had been that CO_2 and NH_3, for example, cross all membranes by dissolving in the lipid phase of the membrane, it is now clear that some membranes are impermeable to CO_2 and NH_3 (Waisbren et al., 1994). Moreover, in many cells, dissolved CO_2 and NH_3 cross the cell membrane via “gas channels” like the aquaporins (AQPs) and Rhesus (Rhs) proteins (Boron, 2010; Cooper and Boron, 1998; Endeward et al., 2008, 2006; Geyer et al., 2013b, 2013c; Holm et al., 2005; Musa-Aziz et al., 2009; Nakhoul et al., 2001, 1998). Moreover, NH_3 can move through the urea transporter UT-B (Geyer et al., 2013a).

Although we have been discussing how transmembrane fluxes of HA and B can affect pH_i, the opposite is also true: pH_i (and pH_o) affect the transmembrane fluxes of HA and B. This principle is particularly important for biological molecules or therapeutic agents (Rodgers and Rowland, 2006; Rodgers et al., 2005) that cross the membrane as neutral weak acids or weak bases. For example, if the drug enters the cell as a weak base, a low pH_i will promote the intracellular reaction $B + H^+ \rightarrow BH^+$. Thus, pH can be extremely important for pharmacokinetics and, if the drug action occurs inside the cell, pharmacodynamics.

2.3.2. Passive fluxes of charged weak acids and bases—Processes that normally can slowly decrease pH_i are the passive influx of H^+ or BH^+, or the passive efflux of A^- (Fig. 5). Under conditions that might prevail in a prototypical cell–a pH_i of 7.20, a pH_o of 7.40, and a transmembrane voltage (V_m) of −60 mV (inside negative)–H^+ would tend to passively enter the cell down its electrochemical gradient. One way of arriving at this conclusion is via the Nernst equation which predicts that the “equilibrium potential” for H^+ is

$$E_{\mathrm{H}} = \frac{2.3RT}{\mathrm{F}} log_{10}\left(\frac{[\mathrm{H}^+]_o}{[\mathrm{H}^+]_i}\right) = \frac{2.3RT}{\mathrm{F}}\left(pH_{\mathrm{i}} - pH_{\mathrm{o}}\right) \cong (58.5 \quad mV)\,(7.2 - 7.4) \cong -12 \quad mV, \tag{7}$$

with R, T and F having their usual meanings. The equilibrium potential for H^+ is the virtual value that V_m would have to be in order for H^+ to be in electrochemical equilibrium across the membrane.

Because V_m is typically more negative than E_H (i.e., the trans-membrane voltage is too negative for H^+ to be in equilibrium), protons tend to passively enter the cell. Assuming a stable V_m and no active (i.e., energy-requiring) transport of H^+, this passive influx of H^+ would continue until pH_i fell to ~6.37, at which point E_H V_m and no further net influx of H^+ would occur. In this example, the influx of H^+ is self-limited and represents an acute intracellular acid load. On the other hand, if the cell has an energy-consuming mechanism to remove H^+ (or accumulate an alkali such as HCO_3^-), pH_i would fall only to the point at which the passive influx of H^+ came into balance with the active efflux of H^+. Here, the passive influx of H^+ represents a continuous or chronic intracellular acid load.

The same electrochemical gradient that moves H^+ into the cell affects the movements of the cationic weak acids BH^+ ($BH^+ \leftrightharpoons B + H^+$, e.g., NH_4^+) and anionic weak bases A^- ($HA \leftrightharpoons A^- H^+$, e.g., HCO_3^-). Let us assume that (a) the neutral species (B or HA) is equilibrated across the plasma membrane (i.e., $[B]_o = [B]_i$, or $[HA]_o = [HA]_i$), (b) the equilibrium ($BH^+ \leftrightharpoons B + H^+$ or $HA \leftrightharpoons A^- + H^+$) holds on both sides of the membrane, and (c) the equilibrium constant is the same on both sides of the membrane. With these three assumptions, one can show that:

For a cationic weak acid ($BH^+ \leftrightharpoons B + H^+$),

$$\frac{[\mathrm{H}^+]_o}{[\mathrm{H}^+]_i} = \frac{[BH^+]_o}{[B\mathrm{H}^+]_i},$$

and that the equilibrium potential for BH^+ equals that for H^+ (i.e., $E_{BH} = E_H$). For an anionic weak base ($HA \leftrightharpoons A^- + H^+$),

$$\frac{[\mathrm{H}^+]_o}{[\mathrm{H}^+]_i} = \frac{[\mathrm{A}^-]_i}{[\mathrm{A}^-]_o},$$

and that the equilibrium potential for A^- equals that for H^+ (i.e., $E_A = E_H$).

Thus, if H^+ tends to passively enter cells, BH^+ will tend to enter passively as well, and A^- will tend to exit passively. In other words, the cell is constantly challenged by intracellular acid loads due to the passive fluxes of the monovalent ionic forms of buffer pairs of the sort discussed above.

The preceding discussion makes no statement about how A^- or BH^+ passively cross the cell membrane. HCO_3^- may move through Cl^- channels (Kaila and Voipio, 1987) and NH_4^+

moves through K^+ channels (Garvin et al., 1988; Kikeri et al., 1992). The right side of Fig. 6 suggests a mechanism for the passive fluxes of H^+, NH_4^+, and HCO_3^- –all occurring via channels.

Here we have been discussing how transmembrane fluxes of A^- and BH^+ can affect pH_i. Conversely, pH_i and pH_o can affect trans-membrane fluxes of A^- and BH^+, which are of importance for biological molecules or therapeutic agents (Rodgers and Rowland, 2006; Rodgers et al., 2005) that cross the membrane as monovalent anions or cations.

2.3.3. Transporters that normally load the cell with acid—As already seen in the previous section, the passive entry of H^+ and of cationic weak acids BH^+ (e.g., NH_4^+), as well as the passive exit of anionic weak bases A^- (e.g., HCO_3^-) all provide a chronic intracellular acid load. The right side of Fig. 6 shows two additional chronic acid-loading mechanisms, transporters that mediate the efflux of HCO_3^- can load the cell with acids. The first is the sub-family of the electrogenic Na/HCO_3 cotransporters (NBCe1 and NBCe2 in the SLC4 family), operating with an apparent Na^+:HCO_3^- stoichiometry of 1:3 (Boron and Boulpaep, 1983; Parker and Boron, 2013; Romero et al., 2013, 1997). The second is the subfamily of $Cl–HCO_3$ (or anion) exchangers (AE1–3 in the SLC4 family; Kopito et al., 1989; Romero et al., 2013; Vaughan-Jones, 1979). In addition, proton-driven transporters can move H^+ into the cell. Examples are the high-affinity glutamate transporters (SLC1 family; Kanai et al., 2013, 1995) and the oligopeptide transporters (SLC15 family; Fei et al., 1994; Smith et al., 2013).

In these examples of carrier-mediated acid-loading mechanisms, H^+ or protonated, cationic weak acids (e.g., BH^+) move in the direction (generally inward) dictated by their electrochemical gradients. Similarly, the deprotonated, anionic weak bases (A^-) move in the direction (generally outward) dictated by their electrochemical gradients. In all cases, the transport is passive from the perspective of acid-base physiology.

2.3.4. Transporters that normally extrude acid from the cell—Unlike acid loaders, acid extruders use energy to move H^+ out of the cell or to move weak bases, such as HCO_3^- , into the cell against their electrochemical gradients. Thus, these transporters are active from the perspective of acid-base physiology. The left side of Fig. 6 lists transporters that normally operate as acid extruders. These include: (1) the Na–H exchanger (NHE, in the SLC9 family; Donowitz et al., 2013; Murer et al., 1976; Orlowski and Grinstein, 2004; Sardet et al., 1989), (2) the electrogenic Na/HCO_3 cotrans-porters (NBCe1, NBCe2 in the SLC4 family; Boron and Boulpaep, 1983; Romero et al., 1997; Virkki et al., 2002) operating with a Na^+:HCO_3^- stoichiometry of 1:2, (3) the electroneutral Na/HCO_3 cotransporters (NBCn1, NBCn2 in the SLC4 family; Choi et al., 2000; Parker et al., 2008; Pushkin et al., 1999) operating with an apparent Na^+:HCO_3^- stoichiometry of 1:1, and (4) the Na^+-driven $Cl–HCO_3$ exchanger (NDCBE in the SLC4 family; Boron and De Weer, 1976a; Boron and Russell, 1983; Russell and Boron, 1976; Grichtchenko et al., 2001; Parker and Boron, 2013; Thomas, 1977). In the above four cases, the energy for exporting H^+ or importing HCO_3^- is the Na^+ electrochemical gradient, in turn established by the Na–K pump, which hydrolyses ATP (Skou, 1957). The Na–K pump is known as a “primary active transporter,” and all of the Na^+- dependent transporters are known as “secondary active transporters.” Another acid

extruder is the vacuolar-type H^+ pump; because it hydrolyzes ATP, it is a primary active transporter. The final acid extruder listed on the left side of Fig. 6 is the unusual voltage-gated H^+ channel Hv1 (DeCoursey, 2013; Ramsey et al., 2006; Sasaki et al., 2006; Thomas and Meech, 1982) that opens only at relatively positive values of V_m, when the electrochemical H^+ gradient is now outward (rather than the normal inward).

2.3.5. The fundamental law of pH_i regulation—We have already reviewed two general mechanisms for chronic intracellular acid loading: (1) passive fluxes of H^+, BH^+, and A^-; and (2) carrier-mediated transport of BH^+ and A^-. To these we can add: (3) cellular metabolism, which generally results in the net production of H^+. Together, these three mechanisms provide an indefinite or continuous acid load at the total rate J_L, tending to lower pH_i. In general, J_L is a function of pH_i and many other parameters. Opposing intracellular acidification are the chronic acid-extruding mechanism–generally working at the expense of energy–that operate at the total rate J_E (Boron, 2004). Like J_L, J_E is generally a function of pH_i and many other parameters.

The fundamental law of pH_i regulation (Bevensee and Boron, 1998; Roos and Boron, 1981) states that the rate of pH_i change is proportional to the difference (J_E–J_L), proportional to the surface to volume ratio (ρ), and inversely proportional to the total intracellular buffering power (β):

$$\frac{dpH_i}{dt} = \frac{\rho}{\beta}(J_E - J_L). \quad (8)$$

If $J_E = J_L$, then $dpH_i/dt = 0$, that is, pH_i is constant in time. If $J_E > J_L$, then $dpH_i/dt > 0$, and pH_i increases with time. Conversely, if $J_E < J_L$, then $dpH_i/dt < 0$, and pH_i decreases with time. Moreover, because dpH_i/dt is proportional to ρ, the rate of pH_i change tends to be greater in smaller cells. Finally, if β approaches zero, the rate of pH_i change approaches $\pm\infty$, regardless of the difference between J_E and J_L, as long as that difference is non-zero. On the other hand, if β approaches ∞, the rate of pH_i change approaches zero (i.e., pH_i is constant), regardless of the difference between J_E and J_L.

An important principle is that steady-state pH_i can change only if the relationship between the pH_i dependencies of J_E and J_L changes. Thus, an acute intracellular acid or alkali load can transiently shift pH_i but cannot, by itself, alter steady-state pH_i. Another corollary is that a change in buffering power cannot, by itself, alter steady-state pH_i–only the rate at which pH_i changes.

2.3.6. Intracellular buffering—In equation (8) we saw that the total intracellular buffering power affects how pH_i changes in time. The total intracellular buffering power is the sum of the buffering powers of all buffer mechanisms, of which we can describe three general types (Roos and Boron, 1981). (1) Physicochemical buffers are weak acids and bases of the form $BH^+ \rightleftharpoons B + H^+$ and $HA \rightleftharpoons A^- + H^+$, discussed above. (2) Biochemical buffers are reactions (e.g., hydrolysis of ATP or of phosphocreatine) that can consume or produce H^+ and are sensitive to pH_i changes in such a way as to minimize pH_i changes. And (3) organellar buffering is the transport of acid-base equivalents across organellar

membranes, resulting in the stabilization of cytosolic pH at the expense of the pH within the organelle.

Chemical buffers are usually divided into two functional groups: intrinsic and extrinsic. Intrinsic buffers (e.g., inorganic phosphate) are those that behave if they are essentially in a closed system, whereas extrinsic buffers (e.g., CO_2/HCO_3^- , NH_3/NH_4^+) are those for which at least one member of the buffer pair behaves as if it were in an open system. Biochemical and organellar buffers are considered intrinsic (Bevensee and Boron, 2013).

Note that buffers tend to minimize changes in pH_i. However, by definition they cannot neutralize an entire acid or alkali load. Hence the need for transporters that adjust their rate to move unbuffered acid-base equivalents across the membrane, tending to stabilize pH_i.

2.4. Interdependence between pH_i and pH_o

2.4.1. Interactions among acid-base equilibria—Regardless of mechanism, any flux of acid-base equivalent–H^+, HA, A^-, B, BH^+–across the cell membrane will perturb all equilibria of intracellular and extracellular pH buffer pairs. The reason is that the reactions involving these buffer pairs all compete for H^+, creating complex interdependencies among buffer reactions, and between pH_i and pH_o.

Imagine a simple case in which pH_i and the pH in the bulk extracellular fluid (BECF) have physiological values, and in which CO_2, a weak base B (e.g., NH_3), and a weak acid HA (e.g., lactic acid, HLac) are permeant, and all are at equilibrium across the cell membrane. If we suddenly raise $[CO_2]_{BECF}$–keeping $[HCO_3^-]_{BECF}$ and pH_{BECF} fixed, using out-of-equilibrium (OOE) CO_2/HCO_3^- technology to make and deliver the solution (Zhao et al., 1995)–the result is a net influx of CO_2 (Fig. 7, flux 1a), followed by all the reaction events (solid black arrows) and diffusion events (dashed black arrows) summarized on the left side of Fig. 7. Among these events are a transient rise in the pH near the outer surface of the cell (pH_S), and a more gradual but sustained fall in pH throughout the cell. The transient rise in pH_S will raise $[B]_S$ (thereby promoting B influx) but will lower $[HA]_S$ (thereby promoting HA efflux). The sustained fall in pH_i will have the opposite effects on intracellular parameters, likewise enhancing the gradient for B influx and HA efflux. Thus, a flux of CO_2 in one direction across the cell membrane will increase the flux of B in the same direction but increase the flux of HA in the opposite direction. We can make comparable statements about situations in which the primary change is a sudden increase in $[B]_{BECF}$ or $[HA]_{BECF}$.

We can also analyze the consequences of suddenly raising $[HCO_3^-]_{BECF}$ (using OOE technology to keep $[CO_2]_{BECF}$ and pH_{BECF} constant), which would cause a net influx of HCO_3^- (Fig. 7, flux 1b) and set into motion the reaction and diffusion events summarize by the gray arrows. The consequences for the other buffer pairs would qualitatively be opposite to what we discussed in the previous paragraph (where we raised $[CO_2]_{BECF}$). What would happen if we simultaneously raised $[HCO_3^-]_{BECF}$ and $[CO_2]_{BECF}$ by the same fractional amount, thereby keeping pH_{BECF} fixed and promoting the influx of both HCO_3^- and CO_2? The influxes of both members of the buffer pair would set up competing tendencies between the processes represented by the black and gray arrow–producing either a rise or a fall in pH_S, depending upon whether the influx of HCO_3^- or CO_2 is dominant. In fact, it is possible

to show that, given any fixed ratio of HCO_3^- and CO_2 influxes, there exists a null pH_{BECF} at which these parallel influxes produce no change in pH_S. Moreover, at pH_{BECF} values above pH_{Null}, the same influxes of HCO_3^- and CO_2 that produced a rise (or a fall) in pH_S when $pH_{BECF} < pH_{Null}$ would have the opposite effect on pH_S.

Of course, it is possible that $[HCO_3^-]_{BECF}$ rises at a fixed $[CO_2]_{BECF}$, causing a rise in pH_{BECF} known as metabolic alkalosis. It is also possible that a transporter increases its rate at which it moves HCO_3^- into the cell at a fixed $[HCO_3^-]_{BECF}$. A further complication in the case of HCO_3^- transport is that preliminary data from our laboratory (Lee et al., 2011) suggest that the actual substrate of the Na^+-coupled HCO_3^- transporters (NCBTs) in Fig. 6 is not HCO_3^- but either carbonate ($HCO_3^- \leftrightharpoons CO_3^= + H^+$) or the sodium carbonate ion pair ($NaCO_3^- \leftrightharpoons CO_3^= + Na^+$).

In all of these examples, changes in CO_2 or HCO_3^- or $CO_3^=$ transport will influence B/BH^+ and A^-/HA equilibria both inside and outside the cell. It is clear that intuition will be of limited value in understanding such systems.

2.4.2. Chronic effects of pH_o on pH_i—Disturbances in any parameter that influences processes summarized in Fig. 6–the parameters include pH_{BECF}, $[HCO_3^-]_{BECF}$, and $[Na^+]_{BECF}$–will alter one or more components of J_E or J_L. For example, a decrease in pH_{BECF} will directly or indirectly cause J_E to decrease and J_L to increase, thereby causing steady-state pH_i to fall. Note that this fall in pH_i occurs not simply because of an increased passive influx of H^+ (which may have only a trivial effect because $[H^+]$ is so low) but because of effects on various transporters, resulting in an altered balance between J_E and J_L.

2.4.3. Effects of cellular metabolism on pH_o—Cellular metabolism, integrated over the entire body in the steady-state, produces the fixed acids that the kidney must excrete to maintain a stable blood pH (see *Whole-body pH regulation*). The transporters on the left side of Fig. 6 extrude this metabolically-generated acid to maintain a stable pH_i. In addition, cells produce CO_2 as the result of aerobic metabolism. In the steady state, the newly produced CO_2 merely diffuses out of the cell–in many cases through gas channel–for its journey to the alveoli for excretion via alveolar ventilation (see *The respiratory system*). Note that the stable CO_2 production, reflected by a stable $[CO_2]_i$, does not represent a chronic acid load. However, a sudden increase in cellular CO_2 production will cause $[CO_2]_i$ to rise, eventually leading to a stable but increased rate of CO_2 diffusion from the cell. The rise in $[CO_2]_i$ produces an acute acid load from which the cell may recover by means of the acid extruders in Fig. 6.

A final example is the cellular production of lactic acid, which occurs during anaerobic metabolism and also in cancer cells (the Warburg effect; Warburg et al., 1927). In the steady state, the cellular production of HLac is balanced by HLac efflux, mediated by a family of monocarboxylate transporters (MCTs; ref. Halestrap, 2013). This efflux of HLac is energetically downhill and, like the efflux of CO_2 in the steady state, does not represent a chronic acid load to the cell. However, a sudden increase in HLac production leads to an increase in $[HLac]_i$, with consequences analogous to those outlined in the previous paragraph for CO_2.

Experimental work by Pouyssegur and Swietach and their colleagues (Chiche et al., 2009; Hulikova et al., 2013; Le Floch et al., 2011; Swietach et al., 2009, 2008), and modeling work by Swietach and his colleagues (Swietach et al., 2009, 2008), has begun to elucidate how the efflux of CO_2 and HLac affect pH in the environment around cancer cells.

3. Mathematical models of acid-base physiology

3.1. A short history

We have seen that, as acid-base equivalents move across the plasma membrane, they alter the local ratios of $[B]/[BH^+]$, and $[A^-]/[HA]$. Thus, the transmembrane flux of any one substance, affects the transmembrane gradients of all the others, creating complicated interdependencies that cannot be understood with the use of intuition only. Moreover, each cell type, depending on its role in the tissue, has its own set of plasma-membrane transporter–each with its unique propertie–to regulate pH_i. Thus, pH_i regulation is not only complex but also diverse. Moreover, the same transporters that regulate pH_i also participate in the transport of HCO_3^- and other solutes across epithelia, and epithelial cells somehow coordinate the activities of these transporters to achieve both pH_i regulation and transepithelial transport.

Because of the complexity and diversity of events underling pH_i regulation, investigators have developed mathematical models to simulate cellular acid-base chemistry and help them to interpret physiological data. Here, we briefly review a few of these models.

The first to develop a mathematical model of cellular acid-base chemistry was Albert Roos in 1975. Based on an approach he introduced earlier (Roos, 1965), Roos developed a steady-state model for the passive efflux of lactate (Lac^-)–the prime mover in his analysi–accompanied by an equal influx of lactic acid. The model guided him in postulating that the cell could achieve a steady state only if the antiparallel fluxes of Lac^-/HLac were accompanied by the active extrusion of H^+ at a rate equal to that of HLac influx (Roos, 1975). One year later, Boron and De Weer created the first model capable of predicting how acid-base fluxes affect the time course of pH_i (Boron and De Weer, 1976b). They proposed a single-compartment model that considered CO_2/HCO_3^- (or NH_3/NH_4^+) diffusion across the cell membrane of a squid axon. This model helped guide the first clear description of active pH_i regulation and what has come to be known as the “ammonium pre-pulse.” In the steady state, this dynamic model of Boron and De Weer collapses to the model of Roos. Also in 1976, Gros et al. developed a steady-state mathematical model, based on the Nernst-Planck equation for the electrodiffusion of ions in a bulk solution, to study the role of CA in facilitating the diffusion of CO_2 in phosphate solutions (Gros et al., 1976).

Others have now developed more sophisticated models, both compartmental (Endeward and Gros, 2005) and spatially distributed (Missner et al., 2008; Swietach et al., 2003; Vaughan-Jones et al., 2002). In 2009, Endeward and Gros proposed a one-dimensional reaction-diffusion model to investigate the effects of intracellular and extracellular unstirred layers on the diffusion of CO_2, HCO_3^- , and H_2O across the RBC membrane (Endeward and Gros, 2009). Recently, Swietach et al. developed reaction-diffusion models of acid-base chemistry to study the role of the cancer-associated extracellular CA IX enzyme in spheroids

(Swietach et al., 2009, 2008), clusters (300 μm in diameter) of thousands of cancer cells (each ~8.6 μm in diameter). Reducing the spheroid to a single homogenized cell 300 μm in diameter, and ignoring diffusion within the volume of the 300-μm spheroid, these authors conclude that CA IX facilitates CO_2 removal by spatially regulating pH_i and pH_o (Swietach et al., 2009, 2008). More recently, Hulikova and Swietach used a modified version of the above mathematical model in which they allow neutral species (e.g., CO_2, NH_3), but not their charged counterparts (e.g., HCO_3^- , NH_4^+), to diffuse within the spheroid (Hulikova and Swietach, 2014).

In the following section we review the most recent mathematical models developed by our team to interpret our physiological data on *Xenopus* oocytes. We will discuss advantages and limitations of these models and how additional modeling needs to be performed to reproduce the details of a real biological cell in the body.

3.2. Mathematical models of a Xenopus oocyte

3.2.1. Motivation—Because of their large size (~1.3 mm in diameter) and propensity for heterologous expression, *Xenopus* laevis oocytes are a powerful physiological tool, widely used for functional studies of membrane proteins. In our laboratory, we use *Xenopus* oocytes to study several families of membrane proteins, including: (1) NCBTs, which are important for pH_i regulation and epithelial acid-base transport (Parker and Boron, 2013), as well as (2) AQPs, (3) Rh proteins, and urea transporters (UTs), which, besides conducting H_2O in the case of most AQPs (Preston et al., 1992), may also conduct CO_2 (Cooper and Boron, 1998; Endeward et al., 2008, 2006; Geyer et al., 2013b; Musa-Aziz et al., 2009; Nakhoul et al., 1998) or NH_3 (Geyer et al., 2013a, 2013b, 2013c; Holm et al., 2005; Musa-Aziz et al., 2009; Nakhoul et al., 2001; Ripoche et al., 2006).

In 2009, Musa-Aziz et al., using a polished liquid-membrane microelectrode to monitor surface pH (pH_S) in oocytes as CO_2 or NH_3 diffuses into the cell, were the first to show that different AQPs and Rh proteins have different relative permeabilities to (i.e., selectivities for) NH_3 vs. CO_2 vs. H_2O (Musa-Aziz et al., 2009). These authors used the maximal excursion in the pH_S transient (ΔpH_S) as a semi-quantitative index of CO_2 or NH_3 permeability. The principle behind their approach is the following. In the case of CO_2, exposing a cell to a solution containing equilibrated CO_2/HCO_3^- leads to a rapid influx of CO_2 (Fig. 8A) that causes pH_i to fall because of the intracellular reaction $CO_2 + H_2O \rightarrow HCO_3^- + H^+$ (Fig. 8B, bottom). At the extracellular side of the membrane, the CO_2 influx creates a CO_2 deficit, which can be replenished by diffusion of CO_2 from the bulk extracellular fluid and by the reaction $HCO_3^- + H^+ \rightarrow CO_2 + H_2O$, occurring near the extracellular surface (Fig. 8A). This reaction causes pH_S to rise rapidly to a peak–at a time when the CO_2 influx is maximal–and then decay as the CO_2 influx wanes (Fig. 8B, top). Thus, ΔpH_S ought to be a semi-quantitative index of maximal CO_2 influx. Indeed, expressing AQPs in oocytes causes a ΔpH_S that is larger than that measured in a control H_2O-injected oocyte (Chen et al., 2010; Endeward et al., 2006; Musa-Aziz et al., 2009; Qin and Boron, 2013).

In the case of NH_3, exposing a cell to a solution containing equilibrated NH_3/NH_4^+ causes a transient fall in pH_S as a result of NH_3 influx (as for "B" on the right side of Fig. 7, blue arrows) and ΔpH_S is a semi-quantitative index of NH_3 permeability.

Although the above oocyte model and experimental protocol are invaluable tools for demonstrating that CO_2 and NH_3 can move through gas channels, its power is limited by the inability to extract values of absolute permeability from pH_S measurements. In order to overcoming this obstacle, our team–through an interdisciplinary collaboration among mathematicians and physiologist–developed a theoretical model of CO_2 influx into a spherical cell (Somersalo et al., 2012) to simulate the pH_i and pH_S measurements of (Endeward et al., 2006; Musa-Aziz et al., 2009), with the ultimate goal of being able to extract absolute permeability values.

3.2.2. A first-generation theoretical model—Fig. 8 illustrates the major features of the mathematical model of (Somersalo et al., 2012). The model assumes that the oocyte is a sphere surrounded by a spherical layer of extracellular unconvected fluid (EUF), which in turn is surrounded by an infinite reservoir of BECF. Because reactions and diffusion are the two physicochemical processes occurring in the experiments of (Endeward et al., 2006; Musa-Aziz et al., 2009), Somersalo et al. designed their model to account for reactions among buffers and diffusion of solutes in both the ICF and EUF. The buffers are the CO_2/HCO_3^- buffer system, described by Equation (1), and an indefinitely large number (ℓ = 1, 2,..., N) of non-CO_2/HCO_3^- buffers of the form $HA_\ell \rightleftharpoons A + A_\ell^- + H^+$, each of which can be mobile or immobile. The model allows implementation of a CA enzyme in different locations, with the ability to specify the enzymatic acceleration factor A. The BECF is an infinite reservoir of pre-equilibrated solution (in which no reactions or diffusion occur) that mimics the bath solution that we continuously deliver during physiological experiments. The BECF communicates with the EUF via diffusion. The plasma membrane is assumed to be infinitely thin and permeable only to CO_2. Note that the model, as it is implemented, could in principle allow any solute to diffuse freely across the plasma membrane. However, because in the experiment of Musa-Aziz et al., CO_2 is essentially the only solute that can move through the plasma membrane, the simulations allow only CO_2 to cross the membrane.

The model assumes spherical radial symmetry, and is described by a coupled system of partial differential equations (PDEs), one for each solute s, of the form

$$\frac{\partial}{\partial t}C_s(t,r) = \underbrace{\frac{1}{r^2}\frac{\partial}{\partial r}\left(D_s(t)\,r^2\frac{\partial}{\partial r}C_s(t,r)\right)}_{\text{Diffusion term}} + \underbrace{\sum_{\ell=-3,\ell\neq 0}^{3} S_{s,\ell}\Phi_\ell}_{\text{Reaction term}}.$$

Here, C_s is the concentration of solute *s*; this concentration changes in time and space (radial distance *r* from the center of the cell) because of diffusion (first term on the right-hand side) and of reactions (second term on the right-hand side). Diffusion events are modeled according to Fick's second law of diffusion and reactions, according to the law of mass

action. D_s is the diffusion coefficient of solute *s*, $S_{s,\lambda}$ are the stoichiometry coefficients and Φ_λ are the reaction fluxes.

After setting appropriate boundary conditions (Somersalo et al., 2012), we solve the PDEs numerically using the method of lines and the stiff MATLAB ode solver ode15s.

The model makes predictions that conform well to physiological observations. It can reproduce qualitatively the shape of the pH_i and pH_S trajectories as CO_2 enters the cell. Moreover, it provides interesting new insights on the dependence of $(dpH_i/dt)_{max}$–the maximal rate of intracellular acidification–as well as ΔpH_S on many parameters, including (1) the width d of the EUF[4] and (2) the permeability of the membrane to CO_2 ($P_{M,CO2}$). In the study of gas channels, one wants to estimate the "true" membrane permeability (i.e., the permeability of the lipid phase, together with associated membrane proteins) and not the empirically measured "apparent" membrane permeability, which includes the contributions from the extra- and intracellular unconvected fluid layers that act as additional diffusion barriers in series with the plasma membrane. For example, as the width of the EUF increases, the apparent membrane resistance to CO_2 diffusion rises in parallel, so that the contribution of the membrane becomes smaller and eventually insignificant.

The simulations predict that as *d* decreases, $(dpH_i/dt)_{max}$ become larger (i.e., pH_i decays faster) and ΔpH_S becomes smaller. These results reveal a competition between reaction and diffusion for the replenishment of CO_2 at the extracellular surface of the plasma membrane during CO_2 influx (Fig. 8C). In simulations, decreasing *d* causes the diffusive flux of CO_2 from the BECF to the membrane to increase, but reduces the contribution of the reactions $HCO_3^- + H^+ \rightarrow H_2CO_3 \rightarrow CO_2 + H_2O$. As a consequence of the smaller contribution of the reaction toward CO_2 replenishment, ΔpH_S becomes smaller. As a consequence of the greater diffusive flux and thus greater overall CO_2 replenishment, the CO_2 influx increases and thus $(dpH_i/dt)_{max}$ becomes larger.

Fig. 9 illustrates another interesting insight from the simulations. Starting from zero, raising $P_{M,CO2}$ causes $(dpH_i/dt)_{max}$ and ΔpH_S at first to rise monotonically in parallel, and then to level off ~2 orders of magnitude before $P_{M,CO2}$ approaches the value predicted from the diffusion constant of CO_2 in water ($D_{M,CO2}$). This is an important conclusion because many investigators in the past have assumed that cell membranes offer no resistance to the diffusion of gases like CO_2. Indeed, this assumption is implicit in August Krogh's pioneering work on O_2 diffusion in tissues (Kreuzer, 1982; Krogh, 1919). However, it is now established that the expression of certain channels (Boron, 2010; Endeward et al., 2008, 2006; Geyer et al., 2013b; Musa-Aziz et al., 2009; Nakhoul et al., 1998) can increase the $(dpH_i/dt)_{max}$ or ΔpH_S produced by exposing a cell to CO_2. Gas channels could not have a measureable effect on these quantities unless the basal membrane permeability to CO_2 were several orders of magnitude below the value predicted from $D_{M,CO2}$. Thus, $(dpH_i/dt)_{max}$ and ΔpH_S are indices of membrane permeability.

[4]The EUF is our implementation of the concept of unstirred layers (ULs). ULs are thin, diffuse, stagnant layers always present near the surface of a solid body immersed in a fluid (Dainty and House, 1966). The thickness of a UL is defined only in the steady state ($\delta_X = D_X/P_X$), may differ for each solute X, and does not take reactions into consideration. Our definition of EUF allows us to establish a precise parameter value throughout a simulation.

In summary, the model of Somersalo et al. makes valuable theoretical predictions and allows extracting information on quantities that one cannot directly measure in physiological experiments (e.g., time and space dependence of concentrations of solutes like CO_2). To our knowledge, none of the current mathematical models of acid-base chemistry include the biological details (competing equilibria among multiple mobile and immobile buffers) and the computational complexity of this reaction-diffusion model. However, even this model needs refinements because it cannot quantitatively reproduce some of the salient features of measured pH_i and pH_S transients. For example, the simulations produce ΔpH_S values that are too small.

3.2.3. Refinements to produce a more realistic oocyte model—Recently, Musa-Aziz et al. used simultaneous measurements of pH_i and pH_S transients to study the effects of the cytosolic enzyme CA II and of the extracellular CA IV (attached to the outer leaflet of the membrane via a GPI linkage) on enhancing transmembrane CO_2 fluxes (Musa-Aziz et al., 2014a, 2014b). They found that (1) injecting CA II into oocytes not only increases $(dpH_i/dt)_{max}$ but also increases ΔpH_S and, (2) expressing CA IV in oocytes not only increases ΔpH_S but also the magnitude of $(dpH_i/dt)_{max}$.

In order to help interpret the data in the two physiological papers noted in the previous paragraph (Musa-Aziz et al., 2014a, 2014b), these authors extended and refined the model of Somersalo et al. These refinements, explained in the third paper in that series (Occhipinti et al., 2014) are the following: (1) reduced water content of cytosol, (2) reduced cytosolic diffusion to account for the viscosity and steric hindrance of the cytoplasm, (3) refined cytosolic CA (i.e., CA II) activity, (4) implementation of a layer of intracellular vesicles beneath the plasma membrane, (5) reduced membrane CO_2 permeability to account for the resistance of the membrane to the movement of CO_2, (6) implementation of folds and microvilli at the plasma membrane, (7) refined extracellular-surface CA (i.e., CA IV) activity, (8) implementation of a vitelline membrane that surrounds the oocyte, and (9) a new more realistic simulation protocol for the delivery and removal of the bulk extracellular CO_2/HCO_3^- solution. With these new features and the appropriate parameter values, the model can approximate the experimentally measured time required for pH_S to reach its peak, the maximal change in pH_S, the time delay (after a change in BECF) before pH_i begins to change at all, and the further lag time before pH_i achieves its maximal rate of descent/all under different sets of experimental conditions.

As noted above, the model allows access to time-dependent concentrations of solutes that cannot be measured in the laboratory. The authors used these concentrations to calculate the transmembrane CO_2 fluxes and all the diffusive and reaction fluxes near the outer and inner side of the membrane. The model predictions confirm the hypothesis that CA II and CA IV enhance transmembrane CO_2 fluxes by producing or consuming CO_2 and thereby maximizing the CO_2 gradient across the membrane.

The model guided the authors in the interpretation and explanation of the data presented in the two physiological papers (Musa-Aziz et al., 2014a, 2014b). An interesting example of the power of mathematical models regards the interpretation of the experiments in which the authors expressed CA IV in oocytes and then examined the effect of intracellular or

extracellular CA inhibitors. The model led to a clear understanding of data that at a first did not seem to make intuitive sense. Further simulations with many different combinations of intracellular and extracellular-surface CA activities predict that, in order to observe the full-blown up effect of extracellular-surface CA activity, a small amount cytosolic CA activity is essential. Conversely, the full effect of cytosolic CA activity requires a small amount of extracellular-surface CA activity. This analysis led to the novel and physiologically important prediction that the effects of simultaneously implementing cytosolic and extracellular-surface CA activity on $(dpH_i/dt)_{max}$ and ΔpH_S are not merely additive, but supra-additive (Fig. 10).

3.2.4. Use of the refined model to study influxes of CO_2 and HCO_3^-, alone or in combination—Here, we exploit our latest version of the oocyte model (Occhipinti et al., 2014) to investigate how the simultaneous in-fluxes of CO_2 and HCO_3^- , as might occur in a physiological experiment, would affect pH_i and pH_S. The blue curves in Fig. 11A, C, E, and G are identical and are the same pH_S waveform that we saw in the top of Fig. 8B. It is the result of a simulation for a control oocyte (i.e., not injected with or expressing any heterologous protein) exposed to 5% CO_2/33 mM HCO_3^- (pH_{BECF} = 7.50), and assumed to be permeable only to CO_2 ($P_{M,CO2} = 3.42 \times 10^{-3}$ cm s^{-1}). Similarly, the blue curves in Fig. 11B, D, F, and H are identical and are the same pH_i waveform that we saw in the bottom of Fig. 8B. Thus, the blue curve in Fig. 11B is the intracellular counterpart to the blue pH_S record in Fig. 11A.

The green curves in Fig. 11A and B are the result of a simulation identical to the one that produced the blue curves, except that here we assume that the oocyte membrane is permeable only to HCO_3^- ($P_{M,HCO3} = 2.27 \times 10^{6-}$ cm s^{-1}; $P_{M,CO2}$ 0). The result is a transient but miniscule fall in pH_S (Fig. 11A) and a slow rise in pH_i (Fig. 11B), reflecting the reactions summarized by the gray arrows and the label “1b” in Fig. 7.

The red curves in Fig. 11A and B are the result of a simulation identical to those that produced the blue and green curves, except that here we assume that the oocyte membrane is permeable both to CO_2 ($P_{M,CO} = 3.42 \times 10^{-3}$ cm s^{-1}) and HCO_3^- (*P*M,HCO = 2.27×10^{-6} cm s^{-1}). For pH_S, the resulting red curve is hardly different from the blue curve (permeability to CO_2 only). However, for pH_i, we now see that the rapid fall in pH_i (caused by the influx of CO_2) is now followed by a slower rise that mimics the pH_i recovery seen in oocytes expressing an NBC with modest activity. The red curve is also similar to the first simulation of pH_i recovery, produced by the two-compartment model of Boron and De Weer (Boron and De Weer, 1976b).

The remaining six panels of Fig. 11 summarize three additional sets of three simulations. In each set, we hold $P_{M,CO2}$ fixed at 3.42×10^{-3} cm s^{-1} but increase $P_{M,HCO3}$ by a factor of 10 compared to the row above it. For the cases in which the membrane is permeable only to HCO_3^- (green lines), we see that increasing $P_{M,HCO3}$ causes the initial decrease in pH_S to become progressively of greater magnitude, with progressively more rapid relaxations (Fig. 11C, E, G). Regarding pH_i, we see that increasing $P_{M,HCO3}$ causes pH_i to rise more rapidly (green lines in Fig. 11D, F, H).

For the cases in which the membrane is permeable both to CO_2 and HCO_3^- (red curves), we see that increasing $P_{M,HCO3}$ causes the pH_S trajectory to have a less positive ΔpH_S (eventually negative) and a faster decay with an undershoot (Fig. 11C, E, G). These trends reflect the increasing dominance of HCO_3^- entry vs. CO_2 entry. Regarding pH_i, we see that increasing $P_{M,HCO3}$ causes the initial rate of pH_i change to become less negative (eventually positive), the pH_i nadir to become increasingly alkaline (eventually absent), and the rate of the late alkalinization to become greater. Again, these trends reflect the increasing dominance of HCO_3^- entry.

Without the mathematical model, one might use intuition to predict the general shapes of the green and blue curves but, of course, not the detailed trajectories. However, even if one were given the green and blue trajectories, intuition would be of limited value in predicting even the general waveforms of the red curves.

4. Future directions

As we have seen, the reaction, diffusion, and transport events underlying pH physiology at the cell, tissue and whole-body levels are complex and diverse, depending on the cell type or tissue. At this stage, although various groups have made significant progress in modeling acid-base events at the cell and multicellular/tissue levels, we are still far away from a comprehensive, time-dependent model of pH physiology, even at the single-cell level. We now have, for a spherical cell, the beginnings of a model (Occhipinti et al., 2014; Somersalo et al., 2012) that can handle a large number of buffer reactions (necessary for handling a large number of transport events). However, this model is clearly incomplete because it lacks some components that are peculiar to the way physiologists perform experiments, and many other components that are intrinsic to the cell.

4.1. The experiment

Being able to model the cell in the context of real–and imperfect–physiological experiments is important because it is only through experiments that we can gather the data that we need to inform and validate our models. In the case of modeling our oocyte experiments, we must still consider the special environment between the pH_S electrode and the oocyte membrane, and the convective flow around the oocyte, both of which will be important for quantitatively reproducing some features of our oocyte pH_i and pH_S physiological data. Modeling these experimental features may also be valuable in providing insights to real-life problems, such as reaction-diffusion events in the small spaces between cells, or convection of blood around a protrusion in a blood-vessel lumen.

4.2. The cell

In order to model pH_i regulation in a living spherical cell, we will need to introduce the movements of acid-base equivalents like those illustrated in Fig. 6. Specifically, we will need to introduce: (1) electrodiffusion for the passive fluxes of charged weak acids and bases (e.g., H^+ or NH_4^+ leaks), (2) simple (e.g., constant fluxes) or sophisticated kinetics for carrier-mediated transporters (e.g., NBCs), and (3) metabolism as a source of acids (e.g., H^+, HLac, CO_2). Additional physiological details include osmosis, cell-volume regulation, other

solute-transport mechanisms (e.g., Na–K pump), and consideration of electrophysiological principles, including the generation of V_m and macroscopic electroneutrality.

4.3. The geometry

Until now, we have considered only a spherical cell. However, cells can have different and complex geometries. For example, RBCs are biconcave disks, and RBC shape can change as the cells move through the capillaries. For RBCs, others have developed model–both compartmental models (Bidani, 1991; Bidani et al., 1978; Cardenas et al., 1998; Endeward and Gros, 2005) and reaction-diffusion models (Coin and Olson, 1979; Endeward and Gros, 2009; Huang and Hellums, 1994; Moll, 1968; Vandegriff and Olson, 1984a, 1984b)–that address gas exchange across the membrane, carriage (i.e., movement of gases along the blood vessel), and acid-base chemistry. Although it is outside the scope of this paper to discuss these models in depth, we note that none of these reaction-diffusion models describe RBCs as biconcave disks in three-dimensional space. They assume that the RBC is a one-dimensional plane sheet, a sphere with radial symmetry, or a cylindrical disk. They often address only steady-state conditions, and are described by only few partial differential equations (PDEs); when more than two, the number of equations is reduced (by making additional assumptions) to make the model mathematically treatable. Kim-Shapiro's group has proposed reaction-diffusion models of RBCs to study NO permeability, and uses finite element methods (FEM) to model the RBC as a biconcave disk. However, these authors include only two PDEs, for NO and Hb (Huang et al., 2007; Jeffers et al., 2005).

Besides spheres (e.g., lymphocytes, soma of neurons) and biconcave discs (RBCs), other cellular geometries that would be of interest would be cuboids (e.g., epithelia, endothelia), cylinders (e.g., rod-shaped bacteria), and spindles (e.g., skeletal and smooth muscle).

In the case of the renal proximal tubule (a cylindrical epithelium, 1 cell thick), we briefly mention the model of a rat proximal tubule developed by Weinstein (Weinstein, 1986) and later refined (Weinstein et al., 2007). This is a four-compartment (i.e., with instantaneous mixing of solutes within each compartment), steady-state model. The four compartments are (1) the cylindrical lumen, (2) the proximal-tubule cells that form the boundary of most of the lumen, (3) the interspace between proximal-tubule cells (and which forms a small part of the boundary of the lumen), and (4) the space around the outside of the tubule (which anatomically would be in indirect contact with the blood). The model assumes that the proximal tubule is a cylinder with axial flow, where the quantities of interest depend on the position along the axis. The model takes into account the fluxes of many solutes across the boundaries of adjacent compartments. Finally, it considers the equilibria (1) $H_2PO_4^- \rightleftharpoons H^+ + HPO_4^=$, (2) $H_2CO_2 \rightleftharpoons H^+ + HCO_2^-$ (formic acid/formate), (3) $NH_4^+ \rightleftharpoons H^+ + NH_3$, and (4) $CO_2 + H_2O \rightleftharpoons H_2CO_3 \rightleftharpoons H^+ + HCO_3^-$ (with the last reaction being catalyzed by carbonic anhydrases).

Finally, we note the necessity of modeling the spatial inhomogeneity of enzymes, such as the carbonic anhydrases.

4.4. The algorithm

More advanced versions of detailed reaction-diffusion models in different geometries would revolutionize the field acid-base physiological chemistry. However, the inclusion of additional features in a model–even one with simple geometry–will make the model more complex mathematically. For example, in our model, the addition of each new solute requires one new reaction-diffusion equation. Moreover, various reaction and diffusion events can have very different temporal and spatial scales, which also contribute to the challenge of solving the problem numerically. Thus, progress in the field will require more advanced and computationally efficient algorithms.

Perhaps these algorithms will need to be created de novo by mathematicians. Or perhaps the approaches already exist in other disciplines, such as mathematics, chemistry, physics, astronomy, meteorology, or economics. How would we know? A problem is that we have a difficulty in communicating among disciplines because we speak different disciplinary languages, attend different meetings, and publish in different journals. The 2013 inter-union meeting on Multi-Scale Systems Biology, sponsored in part by ICSU (the International Council on Science), was a first step in bringing together representatives of at least the various biological disciplines. And this special issue of the journal, of course, is a first step in publishing together.

What further steps could we take to enhance the exchange of ideas across disciplines, and perhaps help each other to solve problems? It would be helpful to promote better interdisciplinary education among scientists, so that we could better speak one another's languages. It would also be desirable to hold additional inter-union systems biology meetings, but in the future to include modelers from disciplines outside biology. The operant term seems to be interdisciplinarity. On the other hand, it is important to build the strength of individual disciplines, because one cannot have strong interdisciplinary research without strong disciplines.

Acknowledgments

Supported by grants from the Office of Naval Research (N00014-11-1-0889) and the National Institutes of Health (DK81567) to W.F.B., who gratefully acknowledges the support of the Myers/Scarpa endowed chair.

References

Bevensee, MO.; Boron, WF. Thermodynamics and physiology of cellular pH regulation.. In: Kaila, K.; Ransom, BR., editors. PH and Brain Function. John Wiley & Sons; 1998. p. 173-194.

Bevensee, MO.; Boron, WF. Seldin and Giebisch's the Kidney. Physiology & Pathophysiology. Academic Press; 2013. Control of intracellular pH.; p. 1773-1835.

Bidani A. Analysis of abnormalities of capillary CO_2 exchange in vivo. J. Appl. Physiol. Bethesda Md. 1991; 1985(70):1686–1699.

Bidani A, Crandall ED, Forster RE. Analysis of postcapillary pH changes in blood in vivo after gas exchange. J. Appl. Physiol. 1978; 44:770–781. [PubMed: 25860]

Boedtkjer E, Aalkjær C. Intracellular pH in the resistance vasculature: regulation and functional implications. J. Vasc. Res. 2012; 49:479–496. http://dx.doi.org/10.1159/000341235. [PubMed: 22907294]

Boron, W. Acid-base physiology.. In: Boron, W.; Boulpaep, E., editors. Medical Physiology. Saunders Elsevier; Philadelphia, PA: 2012a. p. 652-671.

Boron, W. Organization of the respiratory system.. In: Boron, W.; Boulpaep, E., editors. Medical Physiology. Saunders Elsevier; Philadelphia, PA: 2012b. p. 613-629.

Boron, W. Transport of oxygen and carbon dioxide in the blood.. In: Boron, W.; Boulpaep, E., editors. Medical Physiology. Saunders Elsevier; Philadelphia, PA: 2012c. p. 672-684.

Boron WF. Regulation of intracellular pH. Adv. Physiol. Educ. 2004; 28:160–179. http://dx.doi.org/10.1152/advan.00045.2004. [PubMed: 15545345]

Boron WF. Sharpey-Schafer lecture: gas channels. Exp. Physiol. 2010; 95:1107–1130. http://dx.doi.org/10.1113/expphysiol.2010.055244. [PubMed: 20851859]

Boron WF, Boulpaep EL. Intracellular pH regulation in the renal proximal tubule of the salamander. Na-H exchange. J. Gen. Physiol. 1983; 81:29–52. [PubMed: 6833996]

Boron WF, De Weer P. Active proton transport stimulated by CO2/HCO3−, blocked by cyanide. Nature. 1976a; 259:240–241. http://dx.doi.org/10.1038/259240a0. [PubMed: 2874]

Boron WF, De Weer P. Intracellular pH transients in squid giant axons caused by CO_2, NH_3, and metabolic inhibitors. J. Gen. Physiol. 1976b; 67:91–112. [PubMed: 1460]

Boron WF, Russell JM. Stoichiometry and ion dependencies of the intracellular-pH-regulating mechanism in squid giant axons. J. Gen. Physiol. 1983; 81:373–399. [PubMed: 6842177]

Cardenas, V., Jr.; Heming, TA.; Bidani, A. J. Appl. Physiol. Vol. 84. Bethesda Md: 1998. 1985. Kinetics of CO_2 excretion and intravascular pH disequilibria during carbonic anhydrase inhibition.; p. 683-694.

Chen, L-M.; Zhao, J.; Musa-Aziz, R.; Pelletier, MF.; Drummond, IA.; Boron, WF. Cloning and characterization of a zebrafish homologue of human AQP1: a bifunctional water and gas channel.; 299; Am. J. Physiol. Regul. Integr. Comp. Physiol. 2010. p. R1163eR1174http://dx.doi.org/10.1152/ajpregu.00319.2010

Chiche J, Ilc K, Laférriere J, Trottier E, Dayan F, Mazure NM, Brahimi-Horn MC, Pouysségur J. Hypoxia-inducible carbonic anhydrase IX and XII promote tumor cell growth by counteracting acidosis through the regulation of the intracellular pH. Cancer Res. 2009; 69:358–368. http://dx.doi.org/10.1158/0008-5472.CAN-08-2470. [PubMed: 19118021]

Choi I, Aalkjaer C, Boulpaep EL, Boron WF. An electroneutral sodium/bicarbonate cotransporter NBCn1 and associated sodium channel. Nature. 2000; 405:571–575. http://dx.doi.org/10.1038/35014615. [PubMed: 10850716]

Coin JT, Olson JS. The rate of oxygen uptake by human red blood cells. J. Biol. Chem. 1979; 254:1178–1190. [PubMed: 762123]

Cooper GJ, Boron WF. Effect of pCMBS on CO_2 permeability of Xenopus oocytes expressing aquaporin 1 or its C189S mutant. Am. J. Physiol. 1998; 275:C1481eC1486. [PubMed: 9843709]

Dainty J, House CR. Unstirred layers in frog skin. J. Physiol. 1966; 182:66–78. [PubMed: 5937417]

Davenport, HW. The ABC of Acid-base Chemistry: the Elements of Physiological Blood-Gas Chemistry for Medical Students and Physicians. sixth, revised. ed.. University of Chicago Press; Chicago: 1974.

DeCoursey TE. Voltage-gated proton channels: molecular biology, physiology, and pathophysiology of the H(V) family. Physiol. Rev. 2013; 93:599–652. http://dx.doi.org/10.1152/physrev.00011.2012. [PubMed: 23589829]

Donowitz M, Ming Tse C, Fuster D. SLC9/NHE gene family, a plasma membrane and organellar family of Na^+/H^+ exchangers. Mol. Asp. Med. 2013; 34:236–251. http://dx.doi.org/10.1016/j.mam.2012.05.001.

Duckles SP, Rayner MD, Nadel JA. Effects of CO_2 and pH on drug-ainduced contractions of airway smooth muscle. J. Pharmacol. Exp. Ther. 1974; 190:472–481. [PubMed: 4413181]

Endeward V, Cartron J-P, Ripoche P, Gros G. RhAG protein of the Rhesus complex is a CO_2 channel in the human red cell membrane. FASEB J. Off. Publ. Fed. Am. Soc. Exp. Biol. 2008; 22:64–73. http://dx.doi.org/10.1096/fj.07-9097com.

Endeward V, Gros G. Low carbon dioxide permeability of the apical epithelial membrane of guinea-pig colon. J. Physiol. 2005; 567:253–265. http://dx.doi.org/10.1113/jphysiol.2005.085761. [PubMed: 15932894]

Endeward V, Gros G. Extra- and intracellular unstirred layer effects in measurements of CO_2 diffusion across membranesea novel approach applied to the mass spectrometric ^{18}O technique for red

blood cells. J. Physiol. 2009; 587:1153–1167. http://dx.doi.org/10.1113/jphysiol.2008.165027. [PubMed: 19139045]

Endeward V, Musa-Aziz R, Cooper GJ, Chen L-M, Pelletier MF, Virkki LV, Supuran CT, King LS, Boron WF, Gros G. Evidence that aquaporin 1 is a major pathway for CO_2 transport across the human erythrocyte membrane. FASEB J. Off. Publ. Fed. Am. Soc. Exp. Biol. 2006; 20:1974–1981. http://dx.doi.org/10.1096/fj.04-3300com.

Fei YJ, Kanai Y, Nussberger S, Ganapathy V, Leibach FH, Romero MF, Singh SK, Boron WF, Hediger MA. Expression cloning of a mammalian proton-coupled oligopeptide transporter. Nature. 1994; 368:563–566. http://dx.doi.org/10.1038/368563a0. [PubMed: 8139693]

Garvin JL, Burg MB, Knepper MA. Active NH4+ absorption by the thick ascending limb. Am. J. Physiol. 1988; 255:F57eF65. [PubMed: 3394813]

Geyer RR, Musa-Aziz R, Enkavi G, Mahinthichaichan P, Tajkhorshid E, Boron WF. Movement of NH_3 through the human urea transporter B: a new gas channel. Am. J. Physiol. Ren. Physiol. 2013a; 304:F1447eF1457. http://dx.doi.org/10.1152/ajprenal.00609.2012.

Geyer, RR.; Musa-Aziz, R.; Qin, X.; Boron, WF. Relative CO_2/NH_3 selectivities of mammalian Aquaporins 0–9.. Am. J. Physiol. Cell. Physiol.. 2013b. http://dx.doi.org/10.1152/ajpcell.00033.2013

Geyer RR, Parker MD, Toye AM, Boron WF, Musa-Aziz R. Relative CO_2/NH_3 permeabilities of human RhAG, RhBG and RhCG. J. Membr. Biol. 2013c; 246:915–926. http://dx.doi.org/10.1007/s00232-013-9593-0. [PubMed: 24077989]

Giebisch, G.; Windhager, EE. Transport of acids and bases.. In: Boron, WF.; Boulpaep, EL., editors. Medical Physiology. A Cellular and Molecular Approach. Elsevier Saunders; Philadelphia: 2012. p. 851-865.

Grichtchenko II, Choi I, Zhong X, Bray-Ward P, Russell JM, Boron WF. Cloning, characterization, and chromosomal mapping of a human electroneutral Na^+-driven Cl-HCO_3 exchanger. J. Biol. Chem. 2001; 276:8358–8363. http://dx.doi.org/10.1074/jbc.C000716200. [PubMed: 11133997]

Gros G, Moll W, Hoppe H, Gros H. Proton transport by phosphate diffusionea mechanism of facilitated CO_2transfer. J. Gen. Physiol. 1976; 67:773–790. [PubMed: 6619]

Halestrap AP. The SLC16 gene family e structure, role and regulation in health and disease. Mol. Asp. Med. 2013; 34:337–349. http://dx.doi.org/10.1016/j.mam.2012.05.003.

Hasselbalch KA. Die Berechnung der Wasserstoffzahl des Blutes aus der freien und gebundenen Kohlensaüre desselben, und die Sauerstoffbindung des Blutes als Funktion der Wasserstoffzahl. Biochem. Z. 1916; 78:112–144.

Henderson LJ. The theory of neutrality regulation in the animal organism. Am. J. Physiol. e Leg. Content. 1908; 21:427–448.

Holm LM, Jahn TP, Møller ALB, Schjoerring JK, Ferri D, Klaerke DA, Zeuthen T. NH_3 and NH4+ permeability in aquaporin-expressing Xenopus oocytes. Pflüg. Arch. Eur. J. Physiol. 2005; 450:415–428. http://dx.doi.org/10.1007/s00424-005-1399-1.

Huang KT, Huang Z, Kim-Shapiro DB. Nitric oxide red blood cell membrane permeability at high and low oxygen tension. Nitric Oxide Biol. Chem. Off. J. Nitric Oxide Soc. 2007; 16:209–216. http://dx.doi.org/10.1016/j.niox.2006.11.002.

Huang NS, Hellums JD. A theoretical model for Gas transport and acid/base regulation by blood flowing in microvessels. Microvasc. Res. 1994; 48:364–388. http://dx.doi.org/10.1006/mvre.1994.1062. [PubMed: 7731399]

Hulikova A, Harris AL, Vaughan-Jones RD, Swietach P. Regulation of intracellular pH in cancer cell lines under normoxia and hypoxia. J. Cell. Physiol. 2013; 228:743–752. http://dx.doi.org/10.1002/jcp.24221. [PubMed: 22949268]

Hulikova, A.; Swietach, P. Rapid CO_2 permeation across biological membranes: implications for CO_2 venting from tissue.. FASEB J. Off. Publ. Fed. Am. Soc. Exp. Biol. 2014. http://dx.doi.org/10.1096/fj.13-241752

Igawa T, Ishii S, Tachibana T, Maeda A, Higuchi Y, Shimaoka S, Moriyama C, Watanabe T, Takubo R, Doi Y, Wakabayashi T, Hayasaka A, Kadono S, Miyazaki T, Haraya K, Sekimori Y, Kojima T, Nabuchi Y, Aso Y, Kawabe Y, Hattori K. Antibody recycling by engineered pH-dependent

antigen binding improves the duration of antigen neutralization. Nat. Biotechnol. 2010; 28:1203–1207. http://dx.doi.org/10.1038/nbt.1691. [PubMed: 20953198]

Jeffers A, Xu X, Huang KT, Cho M, Hogg N, Patel RP, Kim-Shapiro DB. Hemoglobin mediated nitrite activation of soluble guanylyl cyclase. Comp. Biochem. Physiol. A. Mol. Integr. Physiol. 2005; 142:130–135. http://dx.doi.org/10.1016/j.cbpb.2005.04.016. [PubMed: 15936233]

Jennings ML. Structure and function of the red blood cell anion transport protein. Annu. Rev. Biophys. Biophys. Chem. 1989; 18:397–430. http://dx.doi.org/10.1146/annurev.bb.18.060189.002145. [PubMed: 2660831]

Kaila K, Voipio J. Postsynaptic fall in intracellular pH induced by GABA-activated bicarbonate conductance. Nature. 1987; 330:163–165. http://dx.doi.org/10.1038/330163a0. [PubMed: 3670401]

Kanai Y, Clémençon B, Simonin A, Leuenberger M, Lochner M, Weisstanner M, Hediger MA. The SLC1 high-affinity glutamate and neutral amino acid transporter family. Mol. Asp. Med. 2013; 34:108–120. http://dx.doi.org/10.1016/j.mam.2013.01.001.

Kanai Y, Nussberger S, Romero MF, Boron WF, Hebert SC, Hediger MA. Electrogenic properties of the epithelial and neuronal high affinity glutamate transporter. J. Biol. Chem. 1995; 270:16561–16568. http://dx.doi.org/10.1074/jbc.270.28.16561. [PubMed: 7622462]

Kikeri D, Sun A, Zeidel ML, Hebert SC. Cellular NH4+⁄K+ transport pathways in mouse medullary thick limb of Henle. Regulation by intracellular pH. J. Gen. Physiol. 1992; 99:435–461. http://dx.doi.org/10.1085/jgp.99.3.435. [PubMed: 1588302]

Kolobow T, Gattinoni L, Tomlinson TA, Pierce JE. Control of breathing using an extracorporeal membrane lung. Anesthesiology. 1977; 46:138–141. [PubMed: 13683]

Kopito RR, Lee BS, Simmons DM, Lindsey AE, Morgans CW, Schneider K. Regulation of intracellular pH by a neuronal homolog of the erythrocyte anion exchanger. Cell. 1989; 59:927–937. [PubMed: 2686841]

Kreuzer F. Oxygen supply to tissues: the Krogh model and its assumptions. Experientia. 1982; 38:1415–1426. [PubMed: 7151956]

Krogh A. The number and distribution of capillaries in muscles with calculations of the oxygen pressure head necessary for supplying the tissue. J. Physiol. 1919; 52:409–415. [PubMed: 16993405]

Le Floch R, Chiche J, Marchiq I, Naiken T, Naïken T, Ilc K, Ilk K, Murray CM, Critchlow SE, Roux D, Simon M-P, Pouysségur J. CD147 subunit of lactate/H^+ symporters MCT1 and hypoxia-inducible MCT4 is critical for energetics and growth of glycolytic tumors. Proc. Natl. Acad. Sci. U. S. A. 2011; 108:16663–16668. http://dx.doi.org/10.1073/pnas.1106123108. [PubMed: 21930917]

Lee S-K, Grichtchenko II, Boron WF. Distinguishing HCO3− from CO32− transport by NBCe1-A. FASEB J. 2011; 25

Li J, Sun XC, Bonanno JA. Role of NBC1 in apical and basolateral HCO3− permeabilities and transendothelial HCO3− fluxes in bovine corneal endothelium. Am. J. Physiol. - Cell. Physiol. 2005; 288:C739eC746. http://dx.doi.org/10.1152/ajpcell.00405.2004. [PubMed: 15548570]

Ludwig M-G, Vanek M, Guerini D, Gasser JA, Jones CE, Junker U, Hofstetter H, Wolf RM, Seuwen K. Proton-sensing G-protein-coupled receptors. Nature. 2003; 425:93–98. http://dx.doi.org/10.1038/nature01905. [PubMed: 12955148]

Matsuyama S, Reed JC. Mitochondria-dependent apoptosis and cellular pH regulation. Cell. Death Differ. 2000; 7:1155–1165. http://dx.doi.org/10.1038/sj.cdd.4400779. [PubMed: 11175252]

Missner A, Kügler P, Saparov SM, Sommer K, Mathai JC, Zeidel ML, Pohl P. Carbon dioxide transport through membranes. J. Biol. Chem. 2008; 283:25340–25347. http://dx.doi.org/10.1074/jbc.M800096200. [PubMed: 18617525]

Moll W. The influence of hemoglobin diffusion on oxygen uptake and release by red cells. Respir. Physiol. 1968; 6:1–15. [PubMed: 5727029]

Murer H, Hopfer U, Kinne R. Sodium/proton antiport in brush-border-membrane vesicles isolated from rat small intestine and kidney. Biochem.. J. 1976; 154:597–604. [PubMed: 942389]

Musa-Aziz R, Chen L-M, Pelletier MF, Boron WF. Relative CO_2/NH_3 selectivities of AQP1, AQP4, AQP5, AmtB, and RhAG. Proc. Natl. Acad. Sci. U. S. A. 2009; 106:5406–5411. http://dx.doi.org/10.1073/pnas.0813231106. [PubMed: 19273840]

Musa-Aziz R, Occhipinti R, Boron WF. Evidence from simultaneous intracellular- and surface-pH transients that carbonic anhydrase IV enhances CO_2 fluxes across Xenopus oocyte plasma membranes. Am. J. Physiol. Cell. Physiol. 2014a; 307:C814eC840. http://dx.doi.org/10.1152/ajpcell.00050.2014. [PubMed: 24965590]

Musa-Aziz R, Occhipinti R, Boron WF. Evidence from simultaneous intracellular- and surface-pH transients that carbonic anhydrase II enhances CO_2 fluxes across Xenopus oocytes plasma membranes. Am. J. Physiol. Cell. Physiol. 2014b; 307:C791eC813. http://dx.doi.org/10.1152/ajpcell.00051.2014. [PubMed: 24965587]

Nakhoul NL, Davis BA, Romero MF, Boron WF. Effect of expressing the water channel aquaporin-1 on the CO_2 permeability of Xenopus oocytes. Am. J. Physiol. 1998; 274:C543eC548. [PubMed: 9486145]

Nakhoul NL, Hering-Smith KS, Abdulnour-Nakhoul SM, Hamm LL. Transport of NH3⁄NH4+ in oocytes expressing aquaporin-1. Am. J. Physiol. Ren. Physiol. 2001; 281:F255eF263.

Nakhoul NL, Romero MF, Waheed A, Davis BA, Mullins R, Hageman G, Sly WS, Boron WF. Processing and functional expression of carbonic anhydrase isoforms in Xenopus laevis oocytes. FASEB J. 1996; 10:A88.

Occhipinti R, Musa-Aziz R, Boron WF. Evidence from mathematical modeling that carbonic anhydrase II and IV enhance CO_2 fluxes across Xenopus oocytes plasma membranes. Am. J. Physiol. Cell. Physiol. 2014; 307:C841eC858. http://dx.doi.org/10.1152/ajpcell.00049.2014. [PubMed: 24965589]

Orlowski J, Grinstein S. Diversity of the mammalian sodium/proton exchanger SLC9 gene family. Pflüg. Arch. Eur. J. Physiol. 2004; 447:549–565. http://dx.doi.org/10.1007/s00424-003-1110-3.

Parker MD, Boron WF. The divergence, actions, roles, and relatives of sodium-coupled bicarbonate transporters. Physiol. Rev. 2013; 93:803–959. http://dx.doi.org/10.1152/physrev.00023.2012. [PubMed: 23589833]

Parker MD, Musa-Aziz R, Rojas JD, Choi I, Daly CM, Boron WF. Characterization of human SLC4A10 as an electroneutral Na/HCO_3 cotransporter (NBCn2) with Cl^- self-exchange activity. J. Biol. Chem. 2008; 283:12777–12788. http://dx.doi.org/10.1074/jbc.M707829200. [PubMed: 18319254]

Preston GM, Carroll TP, Guggino WB, Agre P. Appearance of water channels in Xenopus oocytes expressing red cell CHIP28 protein. Science. 1992; 256:385–387. [PubMed: 1373524]

Pushkin A, Abuladze N, Lee I, Newman D, Hwang J, Kurtz I. Cloning, tissue distribution, genomic organization, and functional characterization of NBC3, a new member of the sodium bicarbonate cotransporter family. J. Biol. Chem. 1999; 274:16569–16575. [PubMed: 10347222]

Qin X, Boron WF. Mutation of a single amino acid converts the human water channel aquaporin 5 into an anion channel. Am. J. Physiol. Cell. Physiol. 2013; 305:C663eC672. http://dx.doi.org/10.1152/ajpcell.00129.2013. [PubMed: 23842530]

Ramsey IS, Moran MM, Chong JA, Clapham DE. A voltage-gated proton-selective channel lacking the pore domain. Nature. 2006; 440:1213–1216. http://dx.doi.org/10.1038/nature04700. [PubMed: 16554753]

Ripoche P, Goossens D, Devuyst O, Gane P, Colin Y, Verkman AS, Cartron J-P. Role of RhAG and AQP1 in NH_3 and CO_2 gas transport in red cell ghosts: a stopped-flow analysis. Transfus. Clin. Biol. J. Société Fr. Transfus. Sang. 2006; 13:117–122. http://dx.doi.org/10.1016/j.tracli.2006.03.004.

Rodgers T, Leahy D, Rowland M. Physiologically based pharmacokinetic modeling 1: predicting the tissue distribution of moderate-to-strong bases. J. Pharm. Sci. 2005; 94:1259–1276. http://dx.doi.org/10.1002/jps.20322. [PubMed: 15858854]

Rodgers T, Rowland M. Physiologically based pharmacokinetic modelling 2: predicting the tissue distribution of acids, very weak bases, neutrals and zwitterions. J. Pharm. Sci. 2006; 95:1238–1257. http://dx.doi.org/10.1002/jps.20502. [PubMed: 16639716]

Romero MF, Chen A-P, Parker MD, Boron WF. The SLC4 family of bicarbonate (HCO3−) transporters. Mol. Asp. Med. 2013; 34:159–182. http://dx.doi.org/10.1016/j.mam.2012.10.008.

Romero MF, Hediger MA, Boulpaep EL, Boron WF. Expression cloning and characterization of a renal electrogenic Na+/HCO3− cotransporter. Nature. 1997; 387:409–413. http://dx.doi.org/10.1038/387409a0. [PubMed: 9163427]

Roopenian DC, Akilesh S. FcRn: the neonatal Fc receptor comes of age. Nat. Rev. Immunol. 2007; 7:715–725. http://dx.doi.org/10.1038/nri2155. [PubMed: 17703228]

Roos A. Intracellular pH and intracellular buffering power of the cat brain. Am. J. Physiol. 1965; 209:1233–1246. [PubMed: 5846926]

Roos A. Intracellular pH and distribution of weak acids across cell membranes. A study of D- and L-lactate and of DMO in rat diaphragm. J. Physiol. 1975; 249:1–25. [PubMed: 239228]

Roos A, Boron WF. Intracellular pH. Physiol. Rev. 1981; 61:296–434.

Russell JM, Boron WF. Role of choloride transport in regulation of intra-cellular pH. Nature. 1976; 264:73–74. [PubMed: 12472]

Sardet C, Franchi A, Pouysségur J. Molecular cloning, primary structure, and expression of the human growth factor-activatable Na^+/H^+ antiporter. Cell. 1989; 56:271–280. [PubMed: 2536298]

Sasaki M, Takagi M, Okamura Y. A voltage sensor-domain protein is a voltage-gated proton channel. Science. 2006; 312:589–592. http://dx.doi.org/10.1126/science.1122352. [PubMed: 16556803]

Schneider H-P, Alt MD, Klier M, Spiess A, Andes FT, Waheed A, Sly WS, Becker HM, Deitmer JW. GPI-anchored carbonic anhydrase IV displays both intra- and extracellular activity in cRNA-injected oocytes and in mouse neurons. Proc. Natl. Acad. Sci. U. S. A. 2013; 110:1494–1499. http://dx.doi.org/10.1073/pnas.1221213110. [PubMed: 23297198]

Seldin, DW.; Giebisch, GH. The Regulation of Acid-base Balance. Raven Press; 1989.

Sendroy J, Seelig S, Slyke DDV. Studies of acidosis Xxii. Application of the Henderson-Hasselbalch equation to human urine. J. Biol. Chem. 1934; 106:463–477.

Skou JC. The influence of some cations on an adenosine triphosphatase from peripheral nerves. Biochim. Biophys. Acta. 1957; 23:394–401. http://dx.doi.org/10.1016/0006-3002(57)90343-8. [PubMed: 13412736]

Smith DE, Clémençon B, Hediger MA. Proton-coupled oligopeptide transporter family SLC15: physiological, pharmacological and pathological implications. Mol. Asp. Med. 2013; 34:323–336. http://dx.doi.org/10.1016/j.mam.2012.11.003.

Somersalo E, Occhipinti R, Boron WF, Calvetti D. A reaction-diffusion model of CO_2 influx into an oocyte. J. Theor. Biol. 2012; 309:185–203. http://dx.doi.org/10.1016/j.jtbi.2012.06.016. [PubMed: 22728674]

Sun XC, Bonanno JA. Identification and cloning of the Na/HCO3− cotransporter (NBC) in human corneal endothelium. Exp. Eye Res. 2003; 77:287–295. http://dx.doi.org/10.1016/S0014-4835(03)00150-7. [PubMed: 12907161]

Swietach P, Patiar S, Supuran CT, Harris AL, Vaughan-Jones RD. The role of carbonic anhydrase 9 in regulating extracellular and intracellular pH in three-dimensional tumor cell growths. J. Biol. Chem. 2009; 284:20299–20310. http://dx.doi.org/10.1074/jbc.M109.006478. [PubMed: 19458084]

Swietach P, Wigfield S, Cobden P, Supuran CT, Harris AL, Vaughan-Jones RD. Tumor-associated carbonic anhydrase 9 spatially coordinates intracellular pH in three-dimensional multicellular growths. J. Biol. Chem. 2008; 283:20473–20483. http://dx.doi.org/10.1074/jbc.M801330200. [PubMed: 18482982]

Swietach P, Zaniboni M, Stewart AK, Rossini A, Spitzer KW, Vaughan-Jones RD. Modelling intracellular H^+ ion diffusion. Prog. Biophys. Mol. Biol. 2003; 83:69–100. [PubMed: 12865074]

Thomas RC. The role of bicarbonate, chloride and sodium ions in the regulation of intracellular pH in snail neurones. J. Physiol. 1977; 273:317–338. [PubMed: 23429]

Thomas RC, Meech RW. Hydrogen ion currents and intracellular pH in depolarized voltage-clamped snail neurones. Nature. 1982; 299:826–828. [PubMed: 7133121]

Traynelis, SF. pH modulation of ligand-gated ion channels.. In: Kaila, K.; Ransom, BR., editors. PH and Brain Function. John Wiley & Sons; 1998. p. 417-446.

Vandegriff KD, Olson JS. A quantitative description in three dimensions of oxygen uptake by human red blood cells. Biophys. J. 1984a; 45:825–835. http://dx.doi.org/10.1016/S0006-3495(84)84226-5. [PubMed: 6722268]

Vandegriff KD, Olson JS. The kinetics of O_2 release by human red blood cells in the presence of external sodium dithionite. J. Biol. Chem. 1984b; 259:12609–12618. [PubMed: 6490633]

Vaughan-Jones RD. Regulation of chloride in quiescent sheep-heart Purkinje fibres studied using intracellular chloride and pH-sensitive micro-electrodes. J. Physiol. 1979; 295:111–137. [PubMed: 42779]

Vaughan-Jones RD, Peercy BE, Keener JP, Spitzer KW. Intrinsic H^+ ion mobility in the rabbit ventricular myocyte. J. Physiol. 2002; 541:139–158. [PubMed: 12015426]

Virkki LV, Wilson DA, Vaughan-Jones RD, Boron WF. Functional characterization of human NBC4 as an electrogenic Na+−HCO3− cotransporter (NBCe2). Am. J. Physiol. Cell. Physiol. 2002; 282:C1278eC1289. http://dx.doi.org/10.1152/ajpcell.00589.2001. [PubMed: 11997242]

Waisbren SJ, Geibel JP, Modlin IM, Boron WF. Unusual permeability properties of gastric gland cells. Nature. 1994; 368:332–335. http://dx.doi.org/10.1038/368332a0. [PubMed: 8127367]

Waldmann R, Champigny G, Bassilana F, Heurteaux C, Lazdunski M. A proton-gated cation channel involved in acid-sensing. Nature. 1997; 386:173–177. http://dx.doi.org/10.1038/386173a0. [PubMed: 9062189]

Warburg O, Wind F, Negelein E. The metabolism of tumors in the body. J. Gen. Physiol. 1927; 8:519–530. [PubMed: 19872213]

Weinstein AM. A mathematical model of the rat proximal tubule. Am. J. Physiol. 1986; 250:F860eF873. [PubMed: 3706537]

Weinstein AM, Weinbaum S, Duan Y, Du Z, Yan Q, Wang T. Flow-dependent transport in a mathematical model of rat proximal tubule. Am. J. Physiol. Ren. Physiol. 2007; 292:F1164eF1181. http://dx.doi.org/10.1152/ajprenal.00392.2006.

Winn R, Stothert J, Nadir B, Hildebrandt J. Lung mechanics following aspiration of 0.1 N hydrochloric acid. J. Appl. Physiol. 1983; 55:1051–1056. [PubMed: 6629935]

Zhao J, Hogan EM, Bevensee MO, Boron WF. Out-of-equilibrium CO2⁄HCO3− solutions and their use in characterizing a new K/HCO_3 cotransporter. Nature. 1995; 374:636–639. http://dx.doi.org/10.1038/374636a0. [PubMed: 7715702]

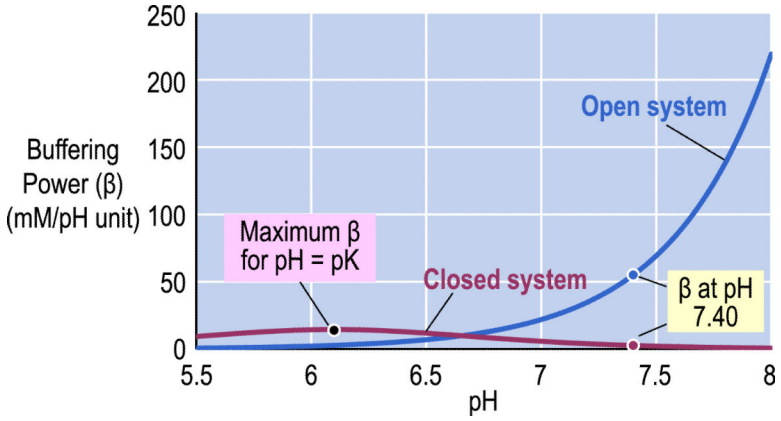

Fig. 1.

pH dependence of buffering power of the carbon dioxide/bicarbonate (CO_2/HCO_3^-) buffer in a fluid having the composition of normal arterial blood. The blue line identifies the buffering power of the CO_2/HCO_3^- buffer in a system that is "open" with respect to CO_2 but closed to HCO_3^- . The purple line identifies the buffering power of the CO_2/HCO_3^- buffer in a system that is "closed" with respect to both CO_2 and HCO_3^- . For the calculations, we assumed that the p*K* of the CO_2/HCO_3^- equilibrium is 6.1, [HCO_3^-] is 24 mM, the solubility of CO_2 is 0.03 mM/mm Hg, and P_{CO2} is 40 mm Hg. Modified from Fig. 28–4 in *Medical Physiology*, 2nd Edition Updated Edition, edited by WF Boron and EL Boulpaep, Philadelphia: Elsevier, 2012.

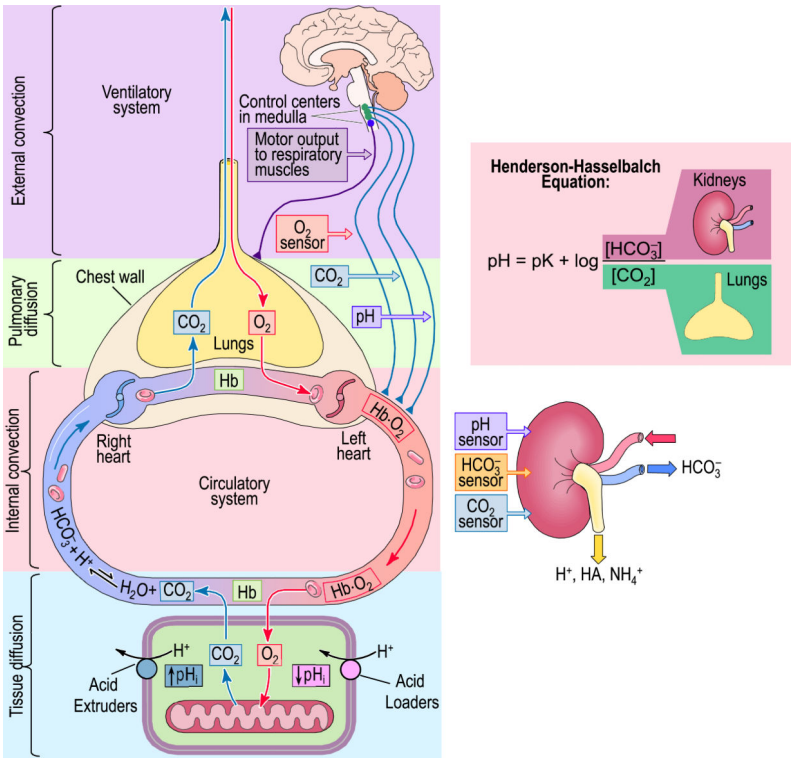

Fig. 2.

The human respiratory and urinary systems and their role in regulating extracellular pH. The respiratory system (main panel) is responsible for removing CO_2 (produced as the result of metabolism) from the body, and in the process controls [CO_2] in the arterial blood. The urinary system (lower right) excretes H^+, acidic buffers ($HA \leftrightharpoons A^- + H^+$), and ammonium ($NH_4^+$), and thereby controls [HCO_3^-] in the arterial blood. Together, the kidney (by controlling [HCO_3^-]) and the lungs (by controlling [CO_2]) control pH, as described by the Henderson-Hasselbalch equation (upper right). Modified from Fig. 26–4 and Fig. 33–7 in *Medical Physiology*, 2nd Edition Updated Edition, edited by WF Boron and EL Boulpaep, Philadelphia: Elsevier, 2012.

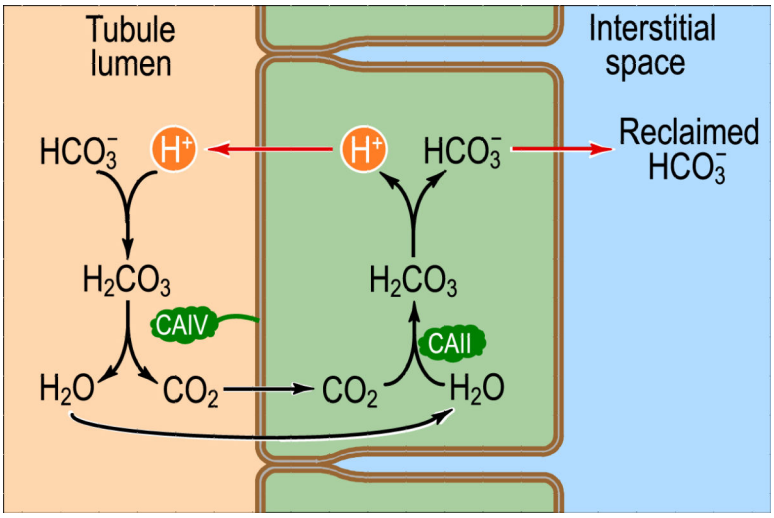

Fig. 3.

Basic cellular mechanism of HCO_3^- reabsorption in the kidneys. The basic unit of the kidney is the nephron, which is basically a tubular epithelium in which a single layer of cells separates the lumen from the interstitial space, which is in direct contact with the blood. By one of several mechanisms (indicated by the red arrow on left), tubule cells can use energy to secrete H^+ into the tubule lumen at various sites along the nephron. One fate of this secreted H^+ is to titrate HCO_3^- that had previously been filtered in the glomerulus. In parallel, the tubule cell uses one of two transport mechanisms (indicated by the red arrow on right) to move HCO_3^- into the interstitial space and ultimately the blood. By this general mechanism, the kidney reclaims virtually all of the filtered HCO_3^- . CAIV and CAII represent the enzymes carbonic anhydrase (CA) II and CA IV. Modified from Fig. 39-2A in *Medical Physiology*, 2nd Edition Updated Edition, edited by WF Boron and EL Boulpaep, Philadelphia: Elsevier, 2012.

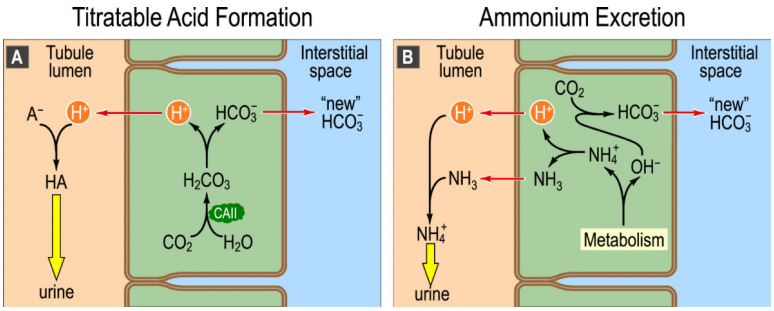

Fig. 4.

Basic cellular mechanism of generation of "new" HCO_3^- . A: Titratable acid formation. At various sites along the nephron, the tubule cells secrete H^+ into the lumen. One result is the titration of weak bases (A^-), filtered from the blood in the glomerulus, to form their conjugate weak acids (HA). In parallel, a new HCO_3^- appears in the interstitial space and then in the blood. B: Ammonium excretion. In the proximal tubule, cells generate ammonia (NH_3) de novo from the amino acids glutamine and glutamate. In the lumen, secreted H^+ titrates this NH_3 to form ammonium (NH_4^+). In parallel, a new HCO_3^- appears in the interstitial space and then in the blood. Because the maximum free $[H^+]$ of the urine is only ~4×10^5 M (pH ~4.4), the urinary excretion of H^+ in the form of HA and NH_4^+–which are typically present at mM level–allows the kidney to eliminate far more acid than it could if all of the secreted protons were excreted in the form of free H^+. Modified from Fig. 39-2B and C in *Medical Physiology*, 2nd Edition Updated Edition, edited by WF Boron and EL Boulpaep, Philadelphia: Elsevier, 2012.

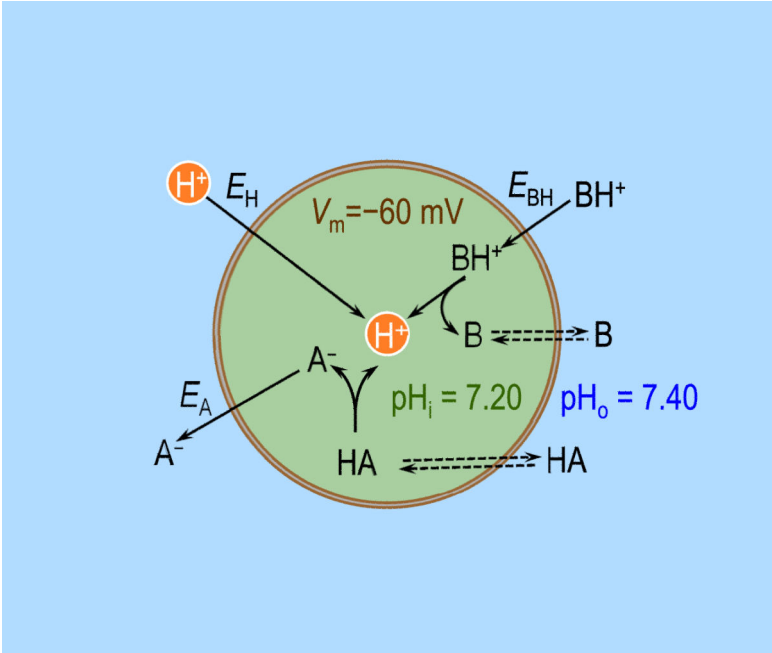

Fig. 5.

Passive fluxes of charged weak acids and bases in a prototypical cell. E_H, E_{BH}, and E_A are the equilibrium membrane potentials, respectively, for H^+, cationic weak acid BH^+, and anionic weak base A^- . Double arrows indicate that the neutral species is equilibrated across the plasma membrane. V_m, membrane potential (referenced to a voltage of zero in the extracellular fluid); pH_i, intracellular pH; pH_o, extracellular pH.

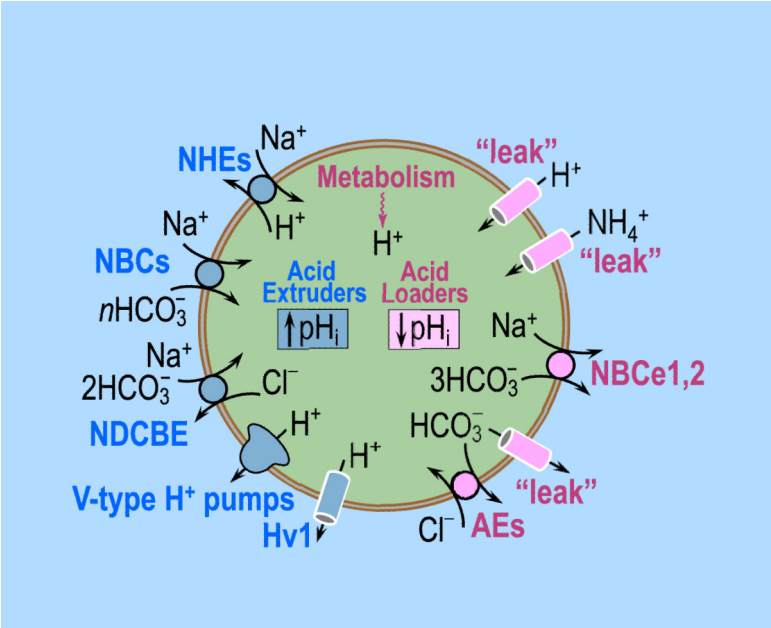

Fig. 6.

A composite of acid extruders and acid loaders in a prototypical cell. Steady-state intracellular pH (pH_i) depends on the balance between the rates of acid extruders and the rates of acid loaders. Acid extruders, listed on the left, are: (1) the Na–H exchangers (NHEs, members of the SLC9 family of solute carriers), (2) the electrogenic Na/HCO_3 cotransporters (NBCe1, NBCe2 in the SLC4 family, n = 2), (3) the electroneutral Na/HCO_3 cotransporters (NBCn1, NBCn2 in the SLC4 family, n 1), (4) the Na^+-driven Cl–HCO_3 exchanger (NDCBE in the SLC4 family), (5) V-type H^+ pumps (fueled by ATP hydrolysis), and (6) the voltage-gated H^+ channel (Hv1). Acid loaders, listed on the right, are: (1) passive fluxes ("leak") of H^+, BH^+ (e.g., NH_4^+) and A^- (e.g., HCO_3^-), (2) the electrogenic Na/HCO_3 cotransporter (NBCe1, NBCe2) operating with a 1:3 stoichiometry (i.e., n = 3), and (3) the Cl–HCO_3 (or anion) exchangers (AE1 –3 in the SLC4 family). Additional acid loaders (not listed) are the proton-driven transporters.

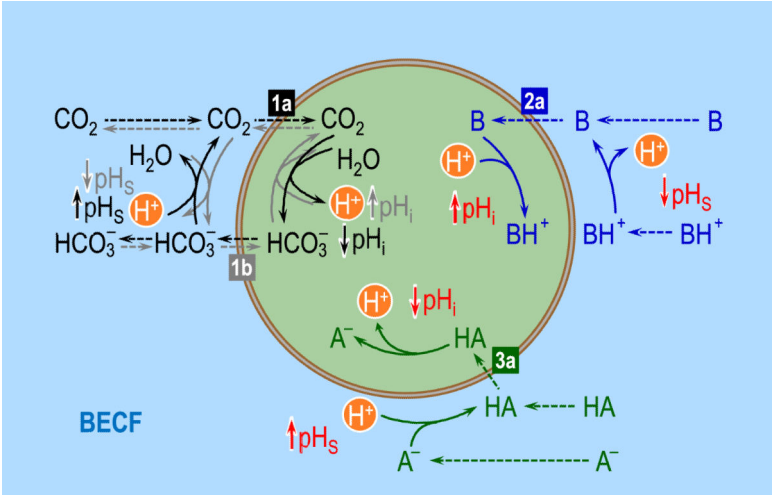

Fig. 7.

Interactions among acid-base equilibria. On the left, the black solid arrows (representing reaction) and dashed arrows (representing diffusion) show the consequences on intracellular (pH_i) and surface pH (pH_S) of the diffusion of CO_2 into the cell (label "1a"), down a CO_2 concentration gradient (i.e., $[CO_2]_o > [CO_2]_i$). The gray arrows show the consequences on pH_i and pH_S of the entry of HCO_3^- into the cell (label "1b"). At the upper right, the blue arrows show the consequences on pH_i and pH_S of the diffusion of a neutral weak base B into the cell ($[B]_o > [B]_i$; label "2a"). Although we do not show the consequences of the entry of BH^+, these would be opposite to those produced by the entry of B. Finally, at the lower right, the green arrows show the consequences on pH_i and pH_S of the diffusion of a neutral weak acid HA into the cell ($[HA]_o > [HA]_i$; label "2a"). Although we do not show the consequences of the entry of BH^+, these would be opposite to those produced by the entry of B. BECF, bulk extra-cellular fluid.

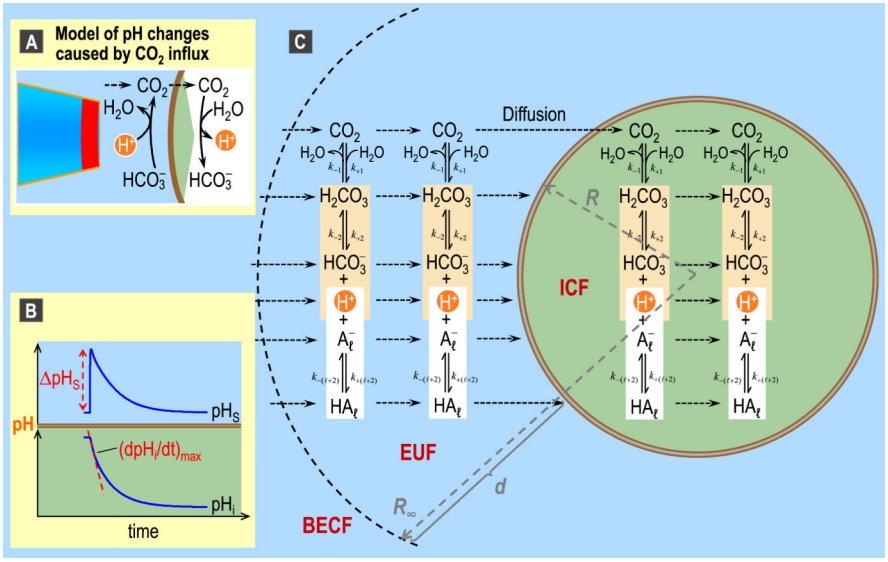

Fig. 8.

pH changes caused by CO_2 influx and major features of the mathematical model of Somersalo et al. (2012). A: Model of acid-base chemistry at the outer surface and inner surface of the plasma membrane as CO_2 enters into the cell. B: Representative intracellular (pH_i) and surface pH (pH_S) transients caused by CO_2 influx. These pH_i and pH_S trajectories are the result of a simulation, and are the same trajectories shown as the blue records in Fig. 11. C: Major components of the mathematical model for a spherical cell with radial symmetry. BECF, bulk extracellular fluid; EUF, extracellular unconvected fluid; ICF, intracellular fluid; *k*, a rate constant. Panel C is modified from Fig. 2 in Somersalo et al. (2012).

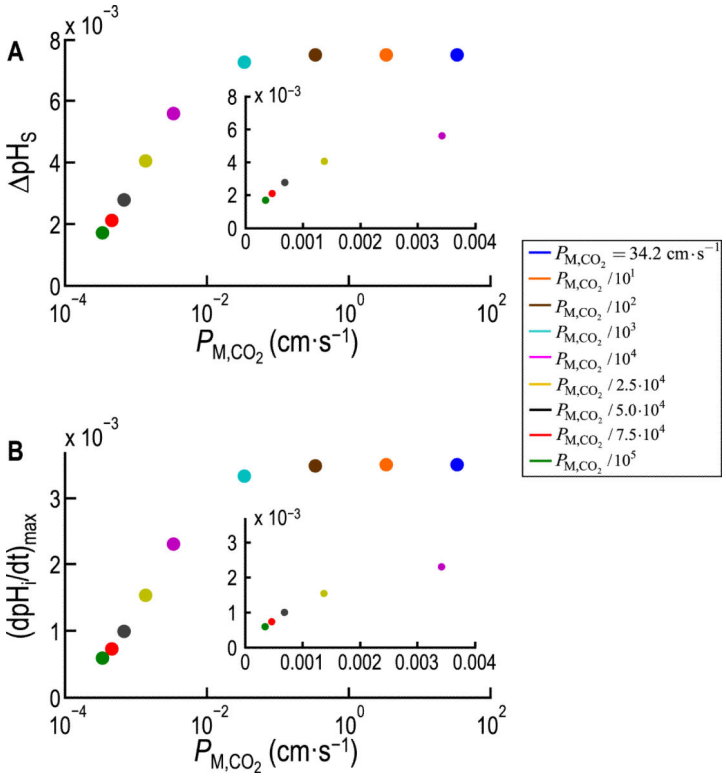

Fig. 9.

Dependence of ΔpH_S and $(dpH_i/dt)_{max}$ on the permeability of the cell membrane to CO_2 ($P_{M,CO2}$), predicted from the model of Somersalo et al. (2012). A: Maximal excursion in the pH_S transient, ΔpH_S (see Fig. 8B, upper), as a function of $P_{M,CO2}$ for nine simulations in which $P_{M,CO2}$ decreases from 34.20 cm s^{-1} (value predicted from the diffusion constant of CO_2 in water) to 34.20×10^{-5} cm s^{-1}. B: Maximal rate of intracellular acidification, $(dpH_i/dt)_{max}$ (see Fig. 8B, lower), as a function of $P_{M,CO2}$ for the same nine simulations reported in A. The two insets are linear re-plots for the five lowest $P_{M,CO2}$ values. Modified from Fig. 7 in Somersalo et al. (2012).

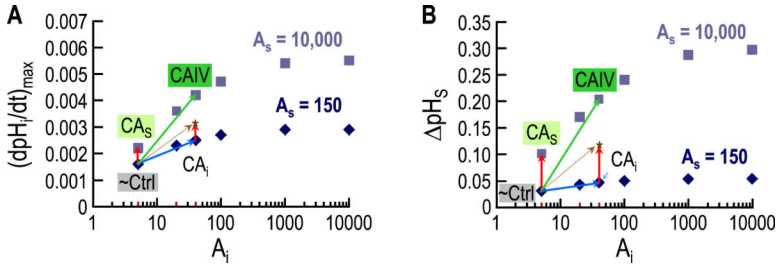

Fig. 10.

Supra-additivity of cytosolic and extracellular-surface CA activities. A: Dependence of $(dpH_i/dt)_{max}$ on the intracellular CA acceleration factor (A_i), for each of two extracellular-surface CA acceleration factors (A_S). The collection of points for each A_S value represents an isopleth, diamonds for A_S = 150 (the baseline or control value), and squares for A_S = 10,000 (expression of an extracellular CA). B: Dependence of ΔpH_S on A_i, for each of the two A_S values. The collections of points for the two isopleths have the same meaning as in panel A. In each panel we show results of 12 simulations (six for each surface CA isopleth) in which we expose a hypothetical oocyte to a BECF solution containing 1.5% CO_2/10 mM HCO_3^- . Each simulation differs because of the values chosen for A_i and A_S. The points labeled "~Ctrl", corresponding to A_i = 5 and A_S = 150, identify a "control" oocyte (i.e., an oocyte not injected or expressing any heterologous protein). The points labeled "CA_S" correspond to a simulation in which we raise A_S from 150 to 10,000 but leave A_i at 5. Note that, compared to "~Ctrl", the CA_S simulation (red vector) predicts a relatively large increase in ΔpH_S but a relatively small increase in $(dpH_i/dt)_{max}$. The points labeled "CA_i" correspond to a simulation in which we raise A_i from 5 to 40 but leave A_S at 150. Note that the CA_i simulation (blue vector) predicts a relatively large rise in $(dpH_i/dt)_{max}$ but a relatively small increase in ΔpH_S. The algebraic sum of the CA_S and CA_i simulations (dashed gold arrow) predicts modest increases in both $(dpH_i/dt)_{max}$ and ΔpH_S. However, the points predicted by the "CAIV" simulation–in which we simultaneously raise A_S from 150 to 10,000 and raise A_i from 5 to 40–reflect substantially larger increases in both $(dpH_i/dt)_{max}$ and ΔpH_S, and mimic the actual physiological data. Thus, the effects of intracellular and surface CA are not merely additive, but supra-additive. Independent evidence indicates that the expression of CA IV in oocytes leads to increases in both surface and intracellular CA IV (Nakhoul et al., 1996; Schneider et al., 2013). Modified from Fig. 13 in (Occhipinti et al., 2014).

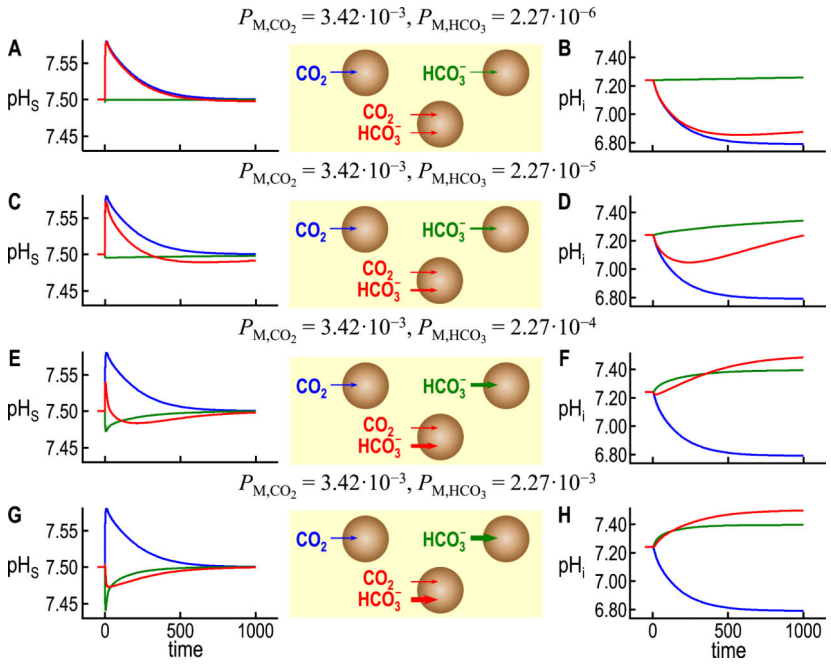

Fig. 11.

Simulations of pH_i and pH_S transients produced by influxes of CO_2 and HCO_3^- alone or in combination. The blue trajectories, which are identical for ΔpH_S in panels A, C, E, and G, and for pH_i in panels B, D, F, and H, are simulations that mimic the exposure of an oocyte to 5% CO_2/33 mM HCO_3^- (pH_o 7.50) when $P_{M,CO2} = 3.42 \times 10^{-}$ cm s^{-1} (the control value from (Occhipinti et al., 2014)) but $P_{M,HCO3} = 0$. The green trajectories in panels A and B are simulations that mimic the exposure of an oocyte to the same CO_2/HCO_3^- solution, but with $P_{M,CO2} = 0$ but $P_{M,HCO3} = 2.27 \times 10^{-}$ cm s^{-1} (estimated from known values of the NBCe1-A current (Lee et al., 2011)). Note that because $P_{M,CO2} = 0$ in these green simulations, the influx of HCO_3^- leads to the formation of intracellular CO_2 that cannot escape from the cell; hence, the relatively small increases in pH_i upon HCO_3^- equilibration across the membrane. In panels C and D, the $P_{M,HCO3}$ values are 10 × greater than in A and B, and the $P_{M,HCO3}$ likewise increase 10 × in E and F, and again in G and H. In each panel, the red trajectories are the predictions for exposing the hypothetical oocyte to CO_2/HCO_3^-, but with $P_{M,CO2} = 3.42 \times 10^{-3}$ cm s^{-1} and $P_{M,HCO3}$ having the same value as the corresponding green trajectory. It is clear that the red trajectories are not merely the algebraic sums of the blue and green trajectories. The red curves in B, D, F, and H all asymptote at $pH_i = 7.50$, reflecting the equilibration of both CO_2 and HCO_3^- across the cell membrane.